Journal of *Marine Science and Engineering*

MDPI

Article

Experimental Modelling of Point-Absorber Wave Energy Converter Arrays: A Comprehensive Review, Identification of Research Gaps and Design of the WECfarm Setup

Timothy Vervaet [1,*], Vasiliki Stratigaki [1], Brecht De Backer [2], Kurt Stockman [2], Marc Vantorre [1] and Peter Troch [1]

[1] Department of Civil Engineering, Ghent University, Technologiepark 60, 9052 Zwijnaarde, Belgium; vicky.stratigaki@ugent.be (V.S.); marc.vantorre@ugent.be (M.V.); peter.troch@ugent.be (P.T.)
[2] Department of Industrial System and Product Design, Ghent University, Graaf Karel de Goedelaan 5, 8500 Kortrijk, Belgium; brecht.db@hotmail.com (B.D.B.); kurt.stockman@ugent.be (K.S.)
* Correspondence: timothy.vervaet@ugent.be; Tel.: +32-9-264-54-89

Abstract: Commercial wave energy exploitation will be realised by placing multiple wave energy converters (WECs) in an array configuration. A point-absorber WEC consists of a floating or submerged body to capture wave energy from different wave directions. This point-absorber WEC acts as an efficient wave absorber that is also an efficient wave generator. Optimising the WEC array layout to obtain constructive interference within the WEC array is theoretically beneficial, whereas for wind farms, it is only important to avoid destructive interference within an array of wind turbines due to wake effects. Moreover, the WEC array layout should be optimised simultaneously with the applied control strategy. This article provides a literature review on the state of the art in physical modelling of point-absorber WEC arrays and the identification of research gaps. To cover the scientific gap of experimental data necessary for the validation of recently developed (nonlinear) numerical models for WEC arrays, Ghent University has introduced the "WECfarm" project. The identified research gaps are translated into design requirements for the "WECfarm" WEC array setup and test matrix. This article presents the design of the "WECfarm" experimental setup, consisting of an array of five generic heaving point-absorber WECs. The WECs are equipped with a permanent magnet synchronous motor (PMSM), addressing the need for WEC array tests with an accurate and actively controllable power take-off (PTO). The WEC array control and data acquisition are realised with a Speedgoat Performance real-time target machine, offering the possibility to implement advanced WEC array control strategies in the MATLAB-Simulink model. Wave basin testing includes long- and short-crested waves and extreme wave conditions, representing real sea conditions. Within the "WECfarm" project, two experimental campaigns were performed at the Aalborg University wave basin: (a) a testing of the first WEC in April 2021 and (b) a testing of a two-WEC array in February 2022. An experimental campaign with a five-WEC array is under preparation at the moment of writing.

Keywords: wave energy converter (WEC); heaving point-absorber WEC; WEC array; WECfarm; physical modelling; real-time control; MATLAB-Simulink

Citation: Vervaet, T.; Stratigaki, V.; De Backer, B.; Stockman, K.; Vantorre M.; Troch, P. Experimental Modelling of Point-Absorber Wave Energy Converter Arrays: A Comprehensive Review, Identification of Research Gaps and Design of the WECfarm Setup. *J. Mar. Sci. Eng.* **2022**, *10*, 1062. https://doi.org/10.3390/jmse10081062

Academic Editor: Unai Fernandez-Gamiz

Received: 29 June 2022
Accepted: 28 July 2022
Published: 2 August 2022

1. Introduction

Wave energy can be extracted from ocean waves by using wave energy converters (WECs) and commercial wave energy will be realised by installing multiple WECs in an array to become economically competitive with other renewable energy resources. A point absorber is a WEC which consists of a floating or submerged body to capture energy from different wave directions. The point absorber's diameter should preferably be in the range of 5–10% of the prevailing wavelength [1]. Due to its ability to absorb energy from different directions, this WEC type is particularly suitable to put in arrays. In a WEC array, hydrodynamic interactions between the WECs occur through the absorption, radiation

and diffraction of waves [2]. Both constructive and destructive interactions occur between individual WECs within a WEC array, called near-field interactions. The power absorption of the entire WEC array reduces the wave height behind the array, called far-field effects. Whether the averaged energy absorbed by each WEC in the array is higher or lower than the energy absorbed by an isolated WEC is defined by the q interaction factor [3]:

$$q = \frac{P}{n \cdot P_s} \tag{1}$$

where P is the total energy absorbed by the WEC array, P_s is the energy absorbed by a single isolated WEC and n is the number of WECs in the array. If wave interactions have a net constructive effect on the absorbed power, q will be larger than unity. If they have a net destructive effect, q will be lower than unity. Therefore, the q interaction factor is widely accepted to quantify near-field interactions (WEC–WEC interactions). This article focuses on the experimental identification of the WEC–WEC and wave–WEC interactions within an array of floating point-absorber WECs.

The layout of the WEC array should be optimised to maximise constructive interactions between the WECs and the power absorption should be improved by applying a control system tailored to the WEC array. In practice, the WEC natural frequency is typically much higher than the ocean wave frequency due to the WEC size constraint [4]. The majority of power produced by WECs occurs during resonant absorption, when the excitation force is in phase with the device velocity. Control strategies aiming to maximise power absorption generally attempt to alter the WEC system dynamics in order to achieve resonance [5]. The control is implemented to act on the WEC power take-off (PTO), the subsystem responsible for the energy transfer from the ocean waves. It is important that the WEC array layout and the control system are optimised simultaneously. A layout optimised without knowledge of the control system can be inferior to the extent of recovering 40% less energy than an array layout optimised with knowledge of the control system [6]. These optimized arrays of interacting WECs can be integrated in a WEC farm. The adopted definitions for a WEC array and a WEC farm in the presented article may differ from the ones used in other research works.

There is a need for available real-life data for the validation of WEC array modelling and optimisation [7]. This is a research gap for the full wave energy sector, not only in the optimisation of WEC arrays. As the computational power capabilities increase yearly, so do the numerical models capabilities, stressing the need for experimental data to validate the models. However, publicly available databases from WEC array experiments are scarce. Only a few physical experiments on arrays of point-absorber WECs have been carried out during the last years and some others were performed around a decade ago [8]. Limited experimental campaigns have been performed due to the high cost of constructing and testing in wave basin facilities, as well as due to the complexity of the experiments and related instrumentation [9].

In the framework of the Hydralab IV WECwakes project coordinated by Ghent University, the near-field interactions and far-field effects have been experimentally investigated for layouts of up to 25 heaving point-absorber type WECs [10–13]. The obtained unique database served for validation purposes of numerical models for studying wave–WEC interactions (near-field interactions) and wave propagation through WEC arrays (far-field effects) [14–17]. Many numerical models have progressively advanced since the completion of the WECwakes project. Therefore, the new experimental "WECfarm" project, introduced by Ghent University and its partners (Queens University Belfast, Aalborg University and University of Vigo) in 2018, aims to deliver a dataset to cover the research gap on the need for publicly available real-life and reliable data to validate these new advanced numerical models. Within the "WECfarm" project, a high-accuracy data acquisition, an actively controllable PTO system and a control platform to implement advanced WEC array control strategies are prioritised. Given the available funding and the complexity of the latter, the number of WECs is limited to five. The WECfarm WEC is intended to be used

only for research purposes and is thus not intended for full-scale deployment. Within the "WECfarm" project, wave basin testing with WEC arrays of up to five real-time controllable heaving point absorbers is planned.

The purpose of this article is threefold. Firstly, Section 2 provides a comprehensive literature review on experimental modelling of point-absorber WEC arrays. Secondly, Section 3 provides the research gaps, resulting from the literature review in Section 2. This Section addresses the motivation for the "WECfarm" project. Thirdly, Section 4 discusses how the design of the "WECfarm" project experimental setup aims to address these research gaps. Therefore, the "WECfarm" WEC is decomposed in its respective subsystems: hydrodynamic, electromechanical, data acquisition system (DAQ) and control platform. This Section addresses the objectives and methodology of the "WECfarm" project. Section 5 provides a discussion and conclusions.

2. Literature Review on Experimental Modelling of Point-Absorber WEC Arrays

The presented literature review considers point-absorber WECs, consisting of a floating or submerged body, named floater or buoy hereafter. For the theoretical background on hydrodynamics of floating structures and on wave energy extraction by point-absorber WEC arrays, the reader is referred to [18,19] and to [20,21], respectively. A theoretical analysis on physical modelling of WECs is presented in [22]. The presented review does not consider point-absorber oscillating water columns (OWC), since their operating principle with a water column oscillating in a plenum and a turbine PTO system can be categorised separately. Gaebele et al. discussed the hydrodynamic interaction within an array of OWCs [23]. Kelly et al. performed experiments with an array of 32 OWCs [24]. Lamont-Kane performed experiments with a single OWC, an array of four OWCs and an array of five OWCs [25]. Doyle et al. performed experiments with a single OWC, an array of three OWCs and a three-chamber OWC [26,27]. A minimum of two WECs is needed to have an array with corresponding WEC–WEC interactions. Within a WEC array, a WEC row refers to a number of WECs placed equidistant to the wavemaker, while a WEC column refers to a number of WECs aligned with the wave propagation direction. For a (j × k)-WEC array, j is the number of columns, while k is the number of rows. As a result, a (1 × k)-WEC array is a column and a (j × 1)-WEC array is a row. The presented review only covers experimental campaigns which have been publicly documented, hence excluding WEC array experiments not disclosed by research institutes or companies. The review is in chronological order, ending with the most recent projects. The focus is on the methodology and research objectives of the performed experiments, rather than on the obtained results. Additionally, the wave testing facility, the design of a single WEC, the tested wave conditions, the number of WECs, the tested WEC separation distances, the WEC array layouts and the target measurements are discussed. In total, 17 WEC array experimental campaigns were identified. Since some campaigns make use of the same WEC model, the number of research projects was reduced to 12. This literature review allows us to identify research gaps in Section 3, which result in unique research objectives and design features of the "WECfarm" project in Section 4.

Pioneering research with WEC arrays was performed by Budal et al. in 1979 [28] and by Count et al. in 1980 [29]. Budal et al. performed experiments on a row of heaving buoys optimised for maximum wave power absorption [28]. The optimum phase was obtained by resonance tuning or by locking the heave motion during controlled intervals of each wave cycle [28]. At a similar time, tests were performed by Count et al. at the University of Edinburgh to measure the q interaction factor of a linear array of both two and ten WECs at different spacings [29]. After these pioneering experimental campaigns, it took some decades until new experiments were set up with point-absorber WEC arrays. The work by Budal et al. and Count et al. is not included in the overview Tables 1–4 due to limited available information on the details of the experiments [28,29].

2.1. Manchester Bobber WEC Array

The first WEC array experimental setup discussed is the Manchester Bobber WEC array. The project was initiated with the purpose to deploy a full-scale WEC array in an ocean environment for power production. Figure 1a shows the employed laboratory-scale model. The only component in contact with the water is a partially immersed axisymmetric floater with a radius a of 0.075 m. The considered scale factor is 1:67. The floater mass m_f is connected to a cable, which is supported by two pulleys. A counterweight of mass m_c applies an opposing force, holding the cable taut and the floater at an equilibrium draft z_{eq} in still water. Both the floater and the counterweight masses can be altered to adjust the draft, the heave and the surge natural frequencies and the hydrodynamic characteristics. In Stallard et al., Thomas et al. and Alexandre et al., a hemisphere-cylinder was considered, while in Weller et al. a flat-bottomed hemisphere-cylinder was considered [30–33]. The pulley nearest to the floater is joined to one side of a freewheel clutch by a shaft. On the other side of the clutch, there is a flywheel providing inertia to the rotating system. The flywheel is connected to a 12 V permanent magnet direct current (PMDC) motor via a flexible coupling. A mechanical torque resists the rotation of the flywheel, thereby applying damping on the system and extracting energy. A motor encoder and code wheel are used to read angular displacements of the motor shaft and pulley, respectively. Changes in the water surface elevation cause the floater to move from its equilibrium position, in a motion similar to water particle orbits. Tethers should ensure only heave motion; however, in order to avoid large horizontal loads on the structure, surge motion has also been allowed for specific extreme wave conditions [34]. Figure 1b shows the experimental setup in the wave flume of Manchester University (5.0 m wide, 18.5 m long and 0.45 m deep).

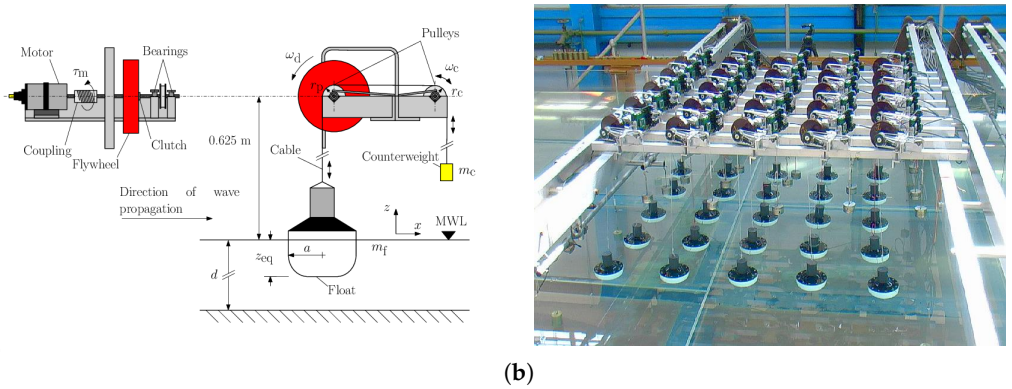

(**a**) (**b**)

Figure 1. Experimental setup of the Manchester Bobber: (**a**) drawing of the WEC model, reprinted with permission from Ref. [34], 2010, Weller and (**b**) picture of the 5 × 5 WEC array in the wave flume of Manchester University, reprinted with permission from Ref. [35], 2008, Manchester University.

Next, the research performed on this setup by Stallard et al., Thomas et al., Alexandre et al. and Weller et al. is discussed [30–33]. Although each time a different number of WECs was considered, the close centre-to-centre spacing equal to four times the WEC radius was retained. Therefore, this array is a closely spaced WEC array, with higher WEC–WEC interactions compared to other research projects discussed later.

Stallard et al. studied the effect of both WEC array size and configuration on the power output and response of individual WECs in the array compared to an isolated WEC [30]. Three configurations were tested: a 1 × 3 column, a 3 × 3 array and a 3 × 4 array. Figure 2a shows the (1 × 3)- and the (3 × 3)-WEC array. Regular waves with an amplitude of 0.013 m and varying frequency were used [30].

Thomas et al. measured values of the WEC free response amplitude for rectilinear (1 × 5)- and (5 × 1)-WEC arrays [31]. Figure 2b shows the tested 1 × 5 column layout and the 5 × 1 row layout. Small scale monochromatic waves with a wave height of 0.026 m and wave periods varying from 0.57 to 1.33 s were applied [31].

Alexandre et al. experimentally measured the transformation of an irregular wave field in the vicinity of a WEC array [32]. Two WEC array configurations were investigated: a single row of five WECs (5 × 1) and a double row of five WECs (5 × 2). Figure 3a shows the tested 5 × 1 row layout. Irregular long-crested waves with a significant wave height of 0.040 m and a peak wave period of 1.31 s were applied. Water surface elevations were measured both before the deployment of the WEC arrays (in an empty wave flume) and with the WEC arrays in place, using a network of three wave gauges installed up- and downwave of the WEC array [32]. The Bretschneider spectrum was constructed with the wave gauge data and used to characterise the influence of the WEC array on the surface elevation.

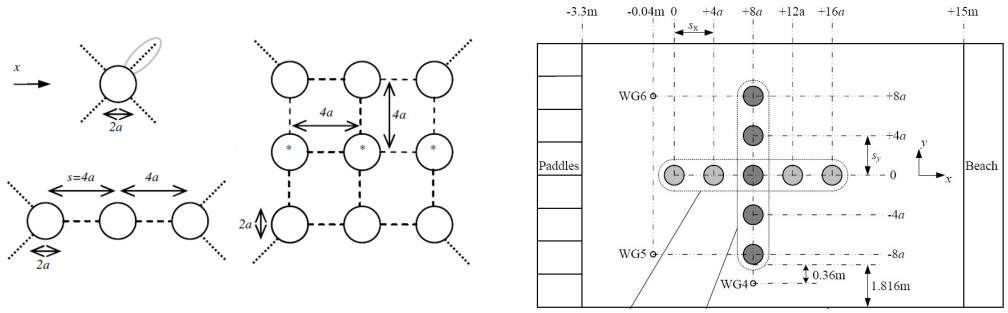

Figure 2. Wave flume of Manchester University's WEC array layout (**a**) used by Stallard et al., adapted with permission from Ref. [30], 2008, Stallard et al. and (**b**) used by Thomas et al., adapted with permission from Ref. [31], 2008, Thomas et al.

Weller et al. experimentally measured the power absorbed by a two-dimensional rectilinear (3 × 4)-WEC array [33]. Figure 3b shows the tested 3 × 4 layout. Regular and irregular long-crested waves with (significant) wave heights varying from 0.015 m to 0.064 m and with (peak) wave periods ranging from 0.61 s to 2.00 s were generated. The capture width, defined as the width of the wave front containing the same available power as the useful power captured by the WEC in the same wave climate, was reported [33].

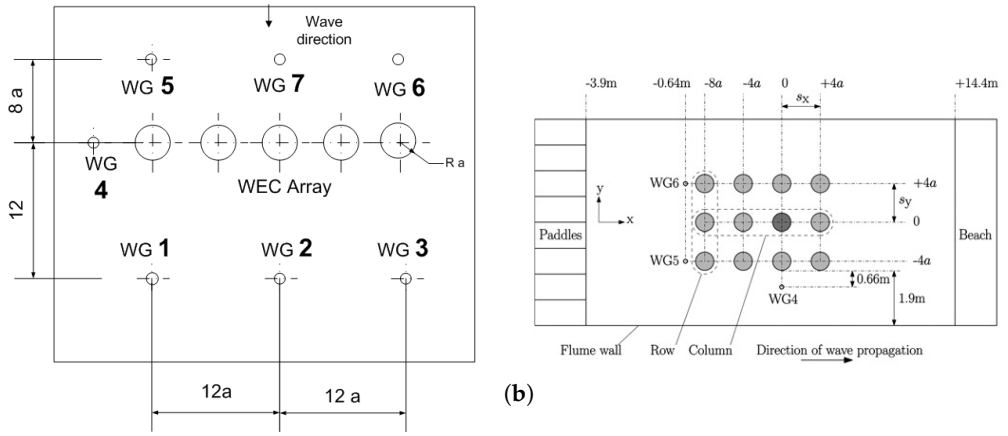

Figure 3. Wave flume of Manchester University' WEC array layout (**a**) used by Alexandre et al., reprinted with permission from Ref. [32], 2009, Alexandre et al. and (**b**) used by Weller et al., reprinted with permission from Ref. [33], 2010, Weller et al.

2.2. PerAWaT Project

The second experimental setup of WEC arrays discussed is the "Performance Assessment of Wave and Tidal array systems" (PerAWaT) project. Child et al. and Folley et al. experimentally tested WEC arrays with 22–24 WECs and Lamont-Kane et al. experimentally tested WEC arrays with four WECs at the Queen's University Belfast (QUB)'s wave

basin in Portaferry, Northern Ireland [36–38]. The wave basin is 18 m long and 16 m wide with a water depth of 0.625 m.

The WEC models had a cylindrical part with 0.25 m diameter, with a hemispherical end and a draft of 0.25 m in still water. A Froude scale factor of 1:80 was applied. The WECs were constrained to move in heave by a pressurised rectilinear air bushing. The heave motion of the WEC was measured using a potentiometer. Power was extracted using a coulomb friction brake, which provides an approximation to a constant pressure hydraulic power take-off. In the physical model, the braking force was adjusted by varying the voltage to a solenoid. The brake force was measured using a cantilever load cell, which measured the combined force due to the clutch and potentiometer [36,37]. Figure 4a shows a drawing of the PerAWaT WEC.

Lamont-Kane et al. experimentally tested WEC arrays with four WECs to assess the primary uncertainties encountered in physical array tests [38]. The sources of uncertainty were described, along with statistical measures used to assess their impact and ensure that the model data collected were of sufficient quality to allow numerical validation [38]. Figure 4b shows the general layout of the setup in the wave basin and Figure 4c shows a picture of the setup.

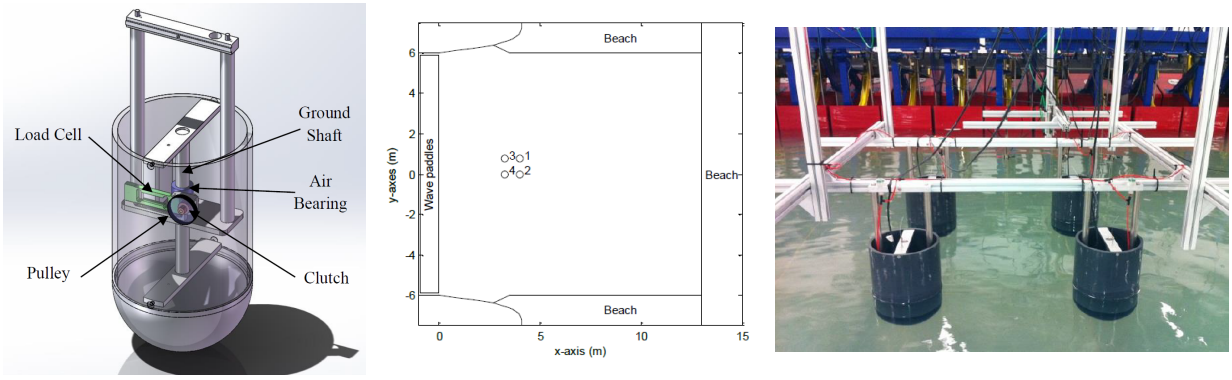

(**a**) (**b**) (**c**)

Figure 4. Experimental setup used by Lamont-Kane et al., reprinted with permission from Ref. [38], 2013, Lamont-Kane et al.: (**a**) WEC model; (**b**) QUB wave basin WEC array layout; (**c**) QUB wave basin setup.

Child et al. used a modified third-generation spectral wave solver (TOMAWAC) to model the power absorption and evolution of wave energy spectra across the WEC array [36]. Folley et al. compared physical model array interactions to those predicted by a spectral-domain numerical model of the WEC array and the suitability of the numerical and physical models was analysed [37]. Both long-crested and short-crested irregular sea states were tested to provide validation for numerical models in real sea conditions. Figure 5a shows the three tested configurations and Figure 5b shows the layout of the second configuration in the wave basin. Figure 5c shows a picture of the setup.

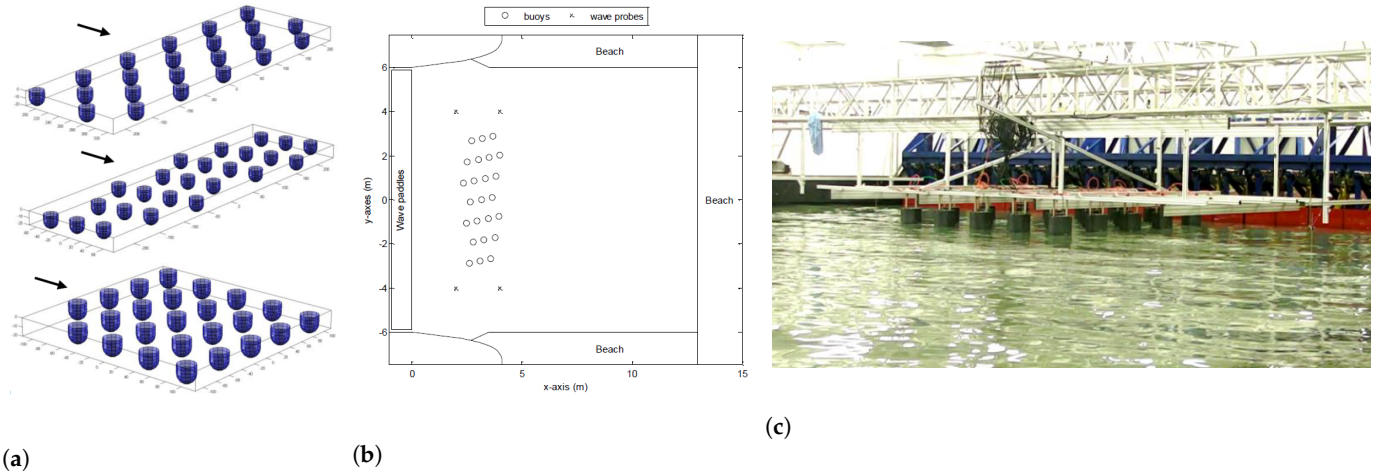

(**a**) (**b**) (**c**)

Figure 5. Experimental setup used by Child et al. and Folley et al., adapted with permission from Ref. [36], 2013, Child et al.: (**a**) three tested configurations; (**b**) QUB wave basin WEC array layout; (**c**) QUB wave basin setup picture.

2.3. Wavebob WEC Array

Mackay et al. compared tests with an array of four Wavebob point-absorber-type WECs on a scale of 1:19 to numerical predictions from a time-domain modelling tool for WECs, called WaveDyn [39]. The tests were executed in the Seakeeping and Manoeuvring basin at MARIN (Wageningen, The Netherlands), which is 170 × 40 m in area and 5 m deep. Similar to the Manchester Bobber and the PerAWaT project, this project was initiated with the aim to deploy a full-scale WEC array in an ocean environment [39].

The Wavebob WEC consists of two bodies: a torus and a central spar, known as the float-neck-tank (FNT). The torus is essentially a wave follower over the range of the wave periods of interest for power conversion, whereas the FNT has a much lower natural period and acts as a source of reference for the motion of the torus. Figure 6a shows four Wavebob WECs on a scale of 1:19. The torus and the FNT are linked via a PTO system, which is modelled using a linear servomotor. At full-scale, the torus has a diameter of 17.60 m, a draft of 4.86 m and a freeboard of 3.00 m. The FNT has a draft of 57.00 m. The PTO is connected to a six-DOF force frame to measure the forces and rotational moments between the torus and FNT. Measurements from the six-DOF frame are used in the control algorithm in order to compensate for friction and stiction in the system. Using this feedback, it was possible to achieve an accurate match to the target PTO profile. The model is moored using three lines spaced at 120° around the model. Each line consists of an anchor line connected to a submerged float which is then connected to a horizontal line section and subsequently to a bridle line arrangement, and finally, to the FNT at two points [39].

The test program comprised radiation tests, where the PTO of one WEC was excited in initially calm water and the effects of the radiated waves on the other WECs were measured, and also tests in regular and irregular long-crested waves. Figure 6b shows the tested diamond layout, with a spacing of 149 m (full-scale) between the model centres, equivalent to 8.5 diameters. Due to the large spacing, this array is not considered a closely spaced WEC array. The waves from 0° correspond to the long-side wave makers and the waves from 90° correspond to the short-side wave makers. The array layout was selected so that adjacent WECs shared anchor points, whilst maintaining a realistic separation distance. Figure 6c shows two Wavebob WECs during a radiation test [39].

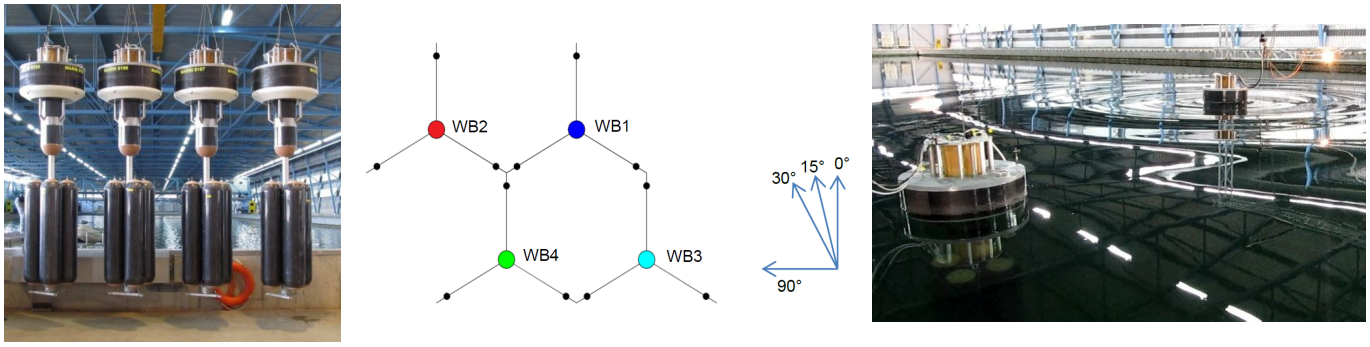

(a) (b) (c)

Figure 6. Experimental setup used by Mackay et al., reprinted with permission from Ref. [39], 2013, Mackay et al.: (**a**) WEC model; (**b**) WEC array layout in the MARIN wave basin; (**c**) MARIN wave basin two-WEC array setup picture.

2.4. WECwakes Project

In the framework of the Hydralab IV WECwakes project, Stratigaki et al. performed experiments on large arrays of up to 25 heaving point-absorber WECs for different geometric rectilinear and staggered WEC array configurations [10–12]. The experiments were performed in the Shallow Water Wave Basin of DHI (Hørsholm, Denmark), which is 35.0 m long and 25.0 m wide, with an overall depth of 0.8 m. These tests were executed with the purpose to investigate near-field interactions and far-field effects and obtain a dataset for numerical modelling validation. Therefore, this project considered a generic WEC concept which was not intended to become commercially deployed in ocean conditions.

Each WEC consisted of a hemisphere-cylinder buoy with a diameter and draft of 0.315 m. The PTO system consisted of polytetrafluoroethylene (PTFE) blocks pressed by springs against a fixed steel shaft, realising damping of the WEC's motion through friction based energy dissipation. Adjusting the length of these springs allows one to adjust the passive damping coefficient, as illustrated on the sketch in Figure 7a. Figure 7b shows a picture of the WECwakes's WEC model. Figure 7c shows a picture of the 5 × 5 rectilinear array setup.

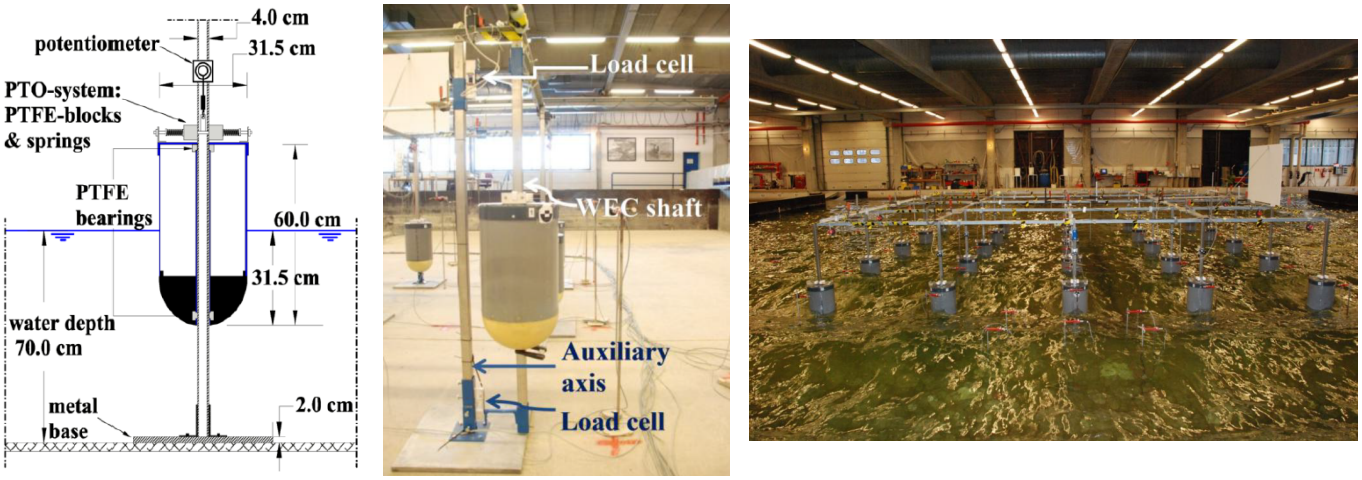

(a) (b) (c)

Figure 7. Experimental setup used by Stratigaki et al., reprinted with permission from Ref. [10], 2014, Stratigaki et al.: (**a**) WEC model; (**b**) WEC model; (**c**) DHI's Shallow Water Wave Basin setup.

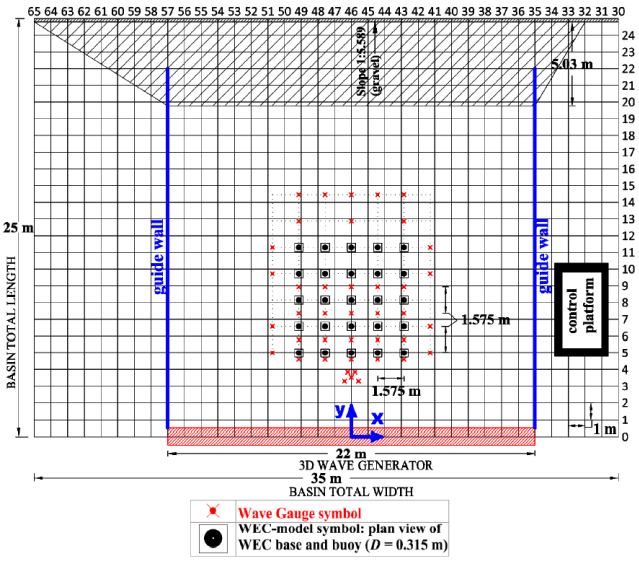

(**a**)

Configuration	Layout sketch	Configuration	Layout sketch
Waves (no WECs)	N/A	10-WEC column	
Individual WEC		5x5-WEC aligned	
2-WEC column		5x5-WEC staggered	
2-WEC row		3x3-WEC aligned 10D	
5-WEC column		3x3-WEC aligned 5D	
5-WEC row		13-WEC staggered	

(**b**)

Figure 8. Experimental setup used by Stratigaki et al., adapted with permission from Ref. [11], 2015, Stratigaki et al.: (**a**) DHI's wave basin 5 × 5 rectilinear WEC array layout; (**b**) sketches of tested WEC (array) configurations at the DHI's wave basin.

A rectilinear arrangement of WEC support structures was employed such that several WEC array configurations could be studied. The configurations tested were: individual WEC, 2-WEC column, 2-WEC row, 5-WEC column, 5-WEC row, 10-WEC array with 2 columns, (5 × 5)-WEC rectilinear array, (5 × 5)-WEC staggered array, (3 × 3)-WEC rectilinear array with a WEC interdistance of 5 D and 10 D and 13-WEC staggered array. Due to the large spacings, these arrays are not considered closely spaced WEC arrays. Figure 8a shows the 5 × 5 rectilinear array layout in the DHI's wave basin and Figure 8b shows the tested configurations. Power absorption tests with regular, panchromatic, long- and short-crested irregular waves were executed. Furthermore, decay tests and wave diffraction tests were executed. The WEC response and modifications of the wave field were measured to provide data for understanding WEC array interactions and to evaluate numerical models of array interaction. Wave gauges were located within and around the WEC array. By extracting spectra at different locations within and around the array, the wave field modifications were studied.

2.5. Wavestar WEC Array

Ruíz et al. performed experiments with a staggered array of five WECs [40] in the deep-water wave basin at Aalborg University (Denmark), which is 15.7 m long, 8.5 m wide, and has a water depth of 0.6 m. The study used experimental data for the validation and uncertainty assessment of the WEC array hydrodynamics tool implemented in DTOcean open-source software, relying on the linearised potential flow theory [40].

The WEC considered for the experiments was a small-scale version of one of the floaters of the Wavestar WEC, reproduced at a scale of 1:20 according to the prototype version of the Wavestar WEC installed in Hanstholm (Denmark) [41]. Figure 9a shows the WEC used in the experiments, consisting of a semisubmerged buoy of 0.254 m diameter and 0.104 m draught connected to a 0.680 m long lever arm.

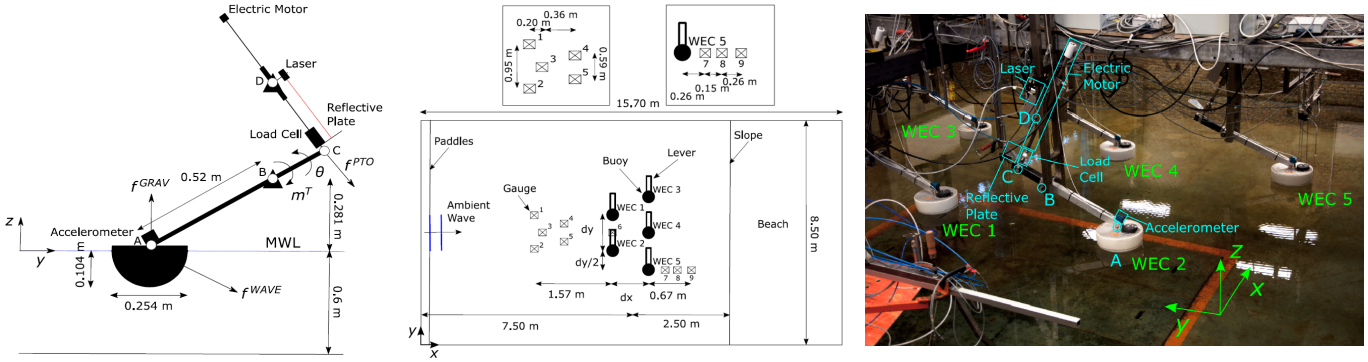

(**a**) (**b**) (**c**)

Figure 9. Experimental setup used by Ruíz et al., adapted with permission from Ref. [40], 2017, Ruíz et al.: (**a**) WEC model; (**b**) Aalborg University wave basin WEC array layout; (**c**) Aalborg University's wave basin setup.

The lever arm was hinged at a height of 0.281 m from the mean water level (MWL) allowing a rotation θ around the x-axis. The WECs were equipped with a linear motor capable of accurately generating linear loads (force directly proportional to velocity), reducing the uncertainty in the physical model [40]. Figure 9b shows the general layout of the setup in the wave basin and Figure 9c shows a picture of the setup. During the experimental campaign only a staggered WEC array was considered with dx = 1.28 m, dy = 1.28 m and a position shift along the y-axis of dy/2 between rows. The WEC array consisted of five WECs split into two rows consisting of two and three WECs, respectively. Diffraction tests with regular waves, radiation tests and power absorption tests with regular and irregular long-crested waves were executed in order to validate the tool. Experimental measurements were then compared with numerical predictions in order to estimate the uncertainty in both wave forces and power absorption [40].

2.6. Australian Maritime College WEC Array

Nader et al. performed array experiments with up to six fully submerged point-absorber WECs moving in six DOFs [9]. The Australian Maritime College's (University of Tasmania) Model Test Basin was used to perform the experiments. The basin is 35 m long, 12 m wide and the water depth was kept constant at 0.6 m. A pit was used to house the linear motor and frame for the active model, such that this equipment was located in the basin floor. The study experimentally investigated the hydrodynamic aspects of an array of generic WECs by separating the problem into its diffraction and radiation problems, removing the need for PTO modelling and control. The experiments measured the interaction factor for two WECs moving in heave and surge. The stereovideogrammetry method was used to measure the wave field around and in the lee of the array [9].

The WECs considered had a generic spherical floater shape. One active model was used for the radiation problem and additional passive models were installed to measure the WEC array interactions when separated at various distances. The passive models were composed of three main components: a vertical post, a hollow sphere and a six-DOF load cell that was fitted between the post and sphere. These custom-built six-DOF load cells measured the hydrodynamic forces and moments experienced by the models during the experiments. The general characteristics of the active model were the same as those of the passive models. However, for the radiation problem, the active model was forced to heave or surge. This behaviour was ruled by an electromagnetic linear motor [9]. Figure 10a shows the active model with the linear motor heave and surge motion configurations.

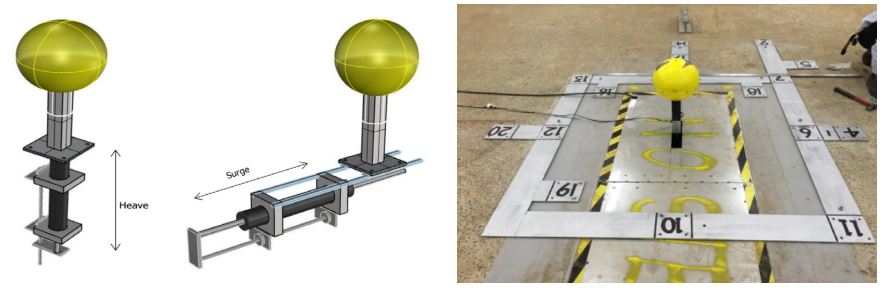

(a) (b)

Figure 10. Experimental setup used by Nader et al., reprinted with permission from Ref. [9], 2017, Nadar et al.: (**a**) active WEC model; (**b**) frame and active WEC.

In order to install and facilitate changes between the different WEC array configurations, a steel positioning frame marking 20 different locations was fixed on the floor of the basin. The frame was positioned in the middle of the tank surrounding the pit where the active model system was installed. The passive models were then fixed at the desired locations for the required configuration. Figure 10b shows this frame and Figure 11a shows the relative locations of the active model and various passive models in the WEC array. Figure 11b shows the various array configurations investigated experimentally. A total of 1447 experimental runs were completed during the experimental campaign. Regular waves were used with wave amplitudes of 0.015 m and 0.030 m and wave frequencies from 0.5 to 1.7 Hz in steps of 0.1 Hz.

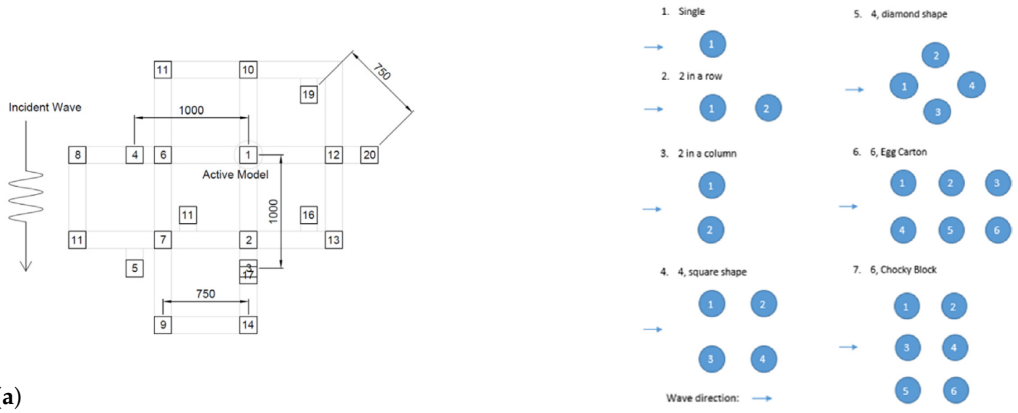

(a) (b)

Figure 11. Experimental setup used by Nader et al., reprinted with permission from Ref. [9], 2017, Nadar et al.: (**a**) WEC array layout; (**b**) sketches of tested WEC array configurations.

2.7. Tu Delft WEC Array

Boere et al. studied experimentally the hydrodynamic interaction of two cylindrical point-absorber WECs in close vicinity [42]. The experiments were performed in the towing tank of TU Delft (The Netherlands), which is 85 m long, 2.75 m wide and 1.20 m deep. The study applied the boundary element method (BEM) model Nemoh and a time-domain WEC Simulator (WEC-Sim) to compute the power output of two WECs while varying their relative position. The trends found in the simulation were experimentally validated by testing scaled versions of two-WEC configurations in the wave tank [42].

To perform the experiments, a generic WEC was identified, namely, an axisymmetric semisubmerged cylinder with a draft of 2.0 m and a diameter of 10.0 m, scaled by a factor of 1:40. The required one-DOF vertical movement of the WECs was secured by mounting the WEC buoy to a rod hanging in linear sliding bearings. The damping of the PTO system

was realised by a viscous damper, with a designed damping coefficient of 80 Ns/m. An elevation sensor was attached to the WEC buoy to accurately measure its vertical position. A load cell was used to connect the piston of the damper to the WEC in order to measure the forces applied by the damper. The combined data of the elevation sensor and the load cell gave insight on both the damper characteristics and the power output of the entire system. Figure 12a shows a rendering of the WEC used in the experiments, with indication of the subsystems.

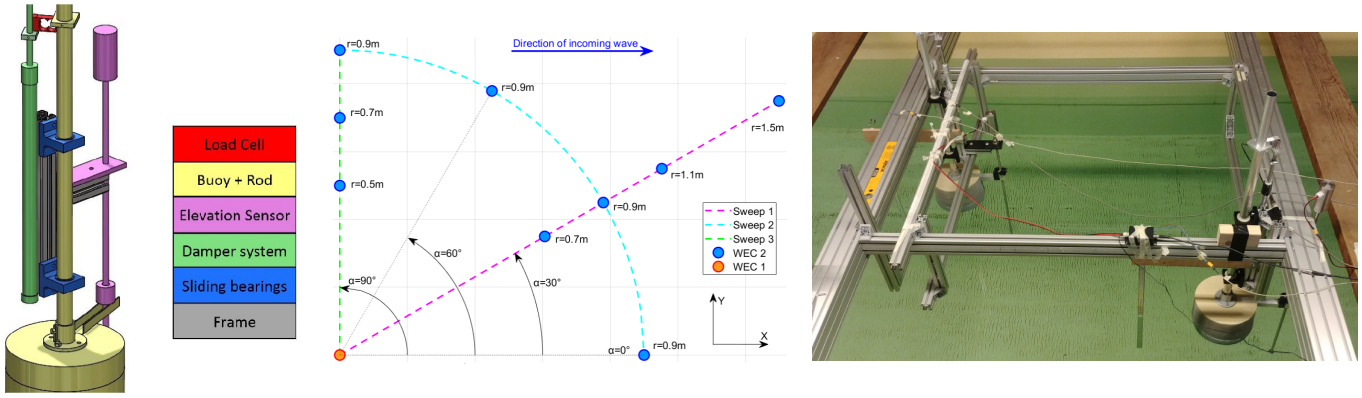

(**a**) (**b**) (**c**)

Figure 12. Experimental setup used by Boere et al., reprinted with permission from Ref. [42], 2018, Boere et al.: (**a**) WEC model; (**b**) tested WEC array configurations; (**c**) TU Delft's towing tank setup picture.

The two WECs were mounted in a frame of sliding aluminium beams, making it easy to adjust the positions of the two WECs in the array. Figure 12c shows the setup of the two-WEC array, where waves are coming from the right. Four regular wave conditions were chosen and correspondingly labelled as weak, fair, moderate and rough. Each wave condition was tested for each of the ten WEC array configurations, resulting in 40 tests. The ten different WEC array configurations consisted of three sweeps as shown in Figure 12b: Sweep 1 with a constant angle of 30° and four different radii, Sweep 2 with a constant radius and four different angles and Sweep 3 with a constant angle of 90° and three different radii. The power output was measured in each of the performed tests [42].

2.8. Multipoint-Absorber WEC

Do et al. experimentally tested a multipoint-absorber WEC (MPAWEC) consisting of ten hemispherical–cylindrical heaving–surging buoys [43]. The research considered a hydrostatic transmission PTO concept with a focus on increasing the absorbed power by smoothing the output power, utilising a common pressure rail connected to a high-pressure accumulator. All of the components of the MPAWEC were mathematically modelled, and simulation results were compared with the experimental results. The test were performed in an ocean wave simulator tank at the Research Institute of Small and Medium Shipbuilding (RIMS), Busan, Korea [43,44]. This project was initiated with the purpose to deploy a full-scale WEC array in an ocean environment for power production.

Figure 13a shows a 3D rendering of the MPAWEC. Ten floating buoys are connected to a moving shaft. A cylinder functioning as a hydraulic pump is attached to each shaft. One end of the cylinder is joined to the moving shaft, while the other is joined to the frame. The frame and all of its attached components are supported by columns, which are fixed to the bottom. The wave excitation force is decomposed into a vertical component and a horizontal component. The resultant force has the same direction as the moving direction of the floating buoy with shaft, or differs from it by a small angle. Therefore, friction between moving parts is reduced, and more power is absorbed from the waves. The piston of the cylinder moves up and down, thereby generating high-pressure fluid at the output port of

the cylinder. The sliding angle of a floating buoy can be adjusted by an actuator, as shown in Figure 13b. The power output was measured during tests with regular waves [43,44].

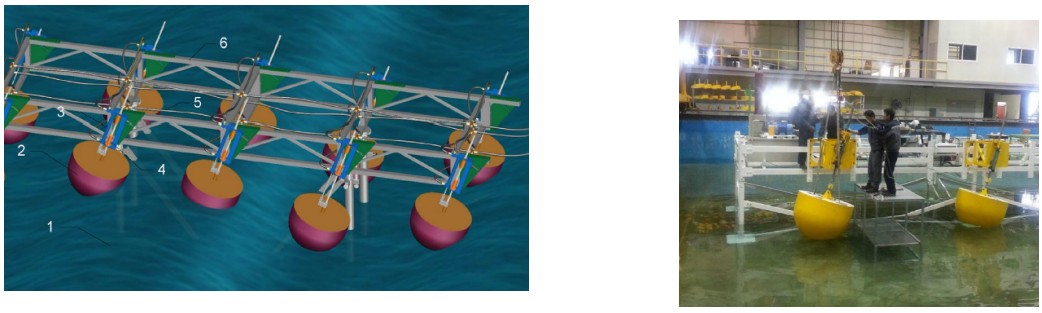

(**a**) (**b**)

Figure 13. Experimental setup used by Do et al., adapted with permission from Ref. [43], 2018, Do et al.: (**a**) 3D rendering of the WEC array layout; (**b**) RIMS's wave basin setup picture.

2.9. Uppsala University's WEC Array

Giassi et al. performed an experimental campaign of arrays with six direct-driven point-absorber WECs. The experimental campaign was carried out in the COAST Lab at the University of Plymouth, UK. The ocean basin is 35 m long and 15.5 m wide, with a moveable floor set to operate at a depth of 2.5 m. The research studied and compared the performances of three different array layouts under several regular and irregular long-crested waves based on the absorbed power. Figure 14b shows the wave basin's WEC array layout of these three configurations.

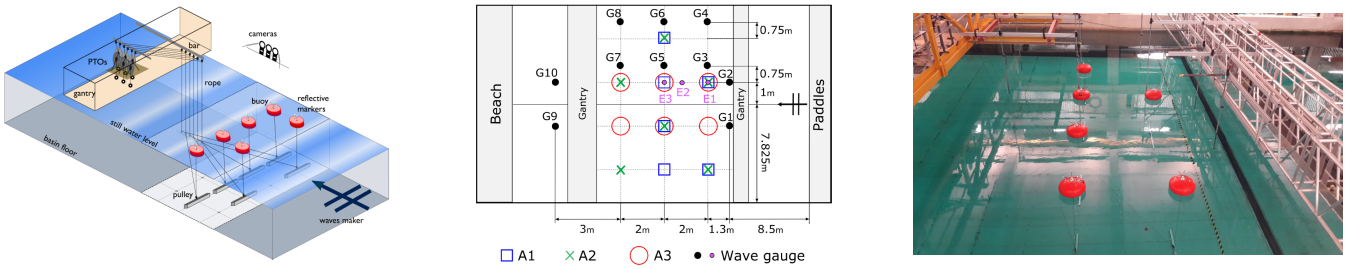

(**a**) (**b**) (**c**)

Figure 14. Experimental setup used by Giassi et al.: (**a**) sketch of the setup's components, reprinted with permission from Ref. [45], 2020, Giassi et al.; (**b**) wave basin WEC array layout, reprinted with permission from Ref. [8], 2019, Giassi et al.; (**c**) the University of Plymouth's COAST Lab setup, reprinted with permission from Ref. [8], 2019, Giassi et al.

It was determined whether the numerical predictions of the best performing array layouts were confirmed by experimental data. The simulations were executed with a frequency-domain model restricted to heave, which was a computationally fast approach that was merged into a genetic algorithm optimisation routine and used to find optimal array configurations [8,45]. The WEC model tested was a 1:10 scaled prototype based on the point-absorber WEC concept developed at Uppsala University (Sweden). Six identical ellipsoidal floating buoys with a diameter of 0.488 m and a height of 0.280 m moving in six DOFs were connected via a system of highly stiff ropes and pulleys to the PTO systems located on the main gantry. Each WEC had a rotating PTO system, and the damping of the PTO was changed by changing the air gap between magnets and an aluminium disc, changing the magnetic flux inside the disc. Additional inertia allowed them to change the WEC natural frequency, allowing to tune the WEC for a specific sea state [46]. Each WEC buoy was equipped with five reflective markers for motion capture, which were tracked by

a set of eight Qualisys six-DOF cameras. Figure 14a shows a sketch of the experimental setup components and Figure 14c shows a picture of the setup at the COAST lab [8,45].

2.10. M4 WEC

The M4 WEC originally consisted of three in-line floaters increasing in diameter (and draft) from bow to stern so that drift forces increased with distance from the floater, causing the WEC to head naturally in the wave direction [47]. Different sizes of floater gave a range of natural periods to enable power capture across a range of wave periods for a given offshore site. Although the M4 WEC was conceived as one single WEC due to the connection between the floaters, the different floaters acted as a WEC array. The floaters cannot be called WECs, since not every floater was equipped with a PTO system. The M4 project was initiated with the purpose of a full-scale ocean deployment for power production. Stansby et al. performed experiments with this M4 WEC with three floaters in the Ocean Wave Basin of the Plymouth COAST laboratory [48,49]. Santo et al. assessed the performance of the three-floater M4 wave energy converter in Albany (on the south coast of western Australia) compared to EMEC in Orkney (UK) based on the experimental data [50]. Moreno et al. conducted an experimental campaign with a six-floater M4 WEC at a scale of 1:50 at the Lir's Ocean Basin at the Beaufort Centre, University College Cork (UCC), Ireland and presented cost estimates for several offshore sites [47]. The basin is 25.0 m by 17.0 m and 1.0 m deep. Liao et al. theoretically analysed the linear hydrodynamic model of the M4 WEC with eight floaters and four PTO units in a state-space form to make it possible to implement advanced control algorithms in real time [51]. Since testing of the M4 WEC resulted in gradual model improvements, only the latest testing by Moreno et al. is included in the presented literature overview [47]. Figure 15a shows a sectional drawing of the six-floater M4 WEC with dimensions and indication of the PTO system with two linear actuators and the mooring line connection.

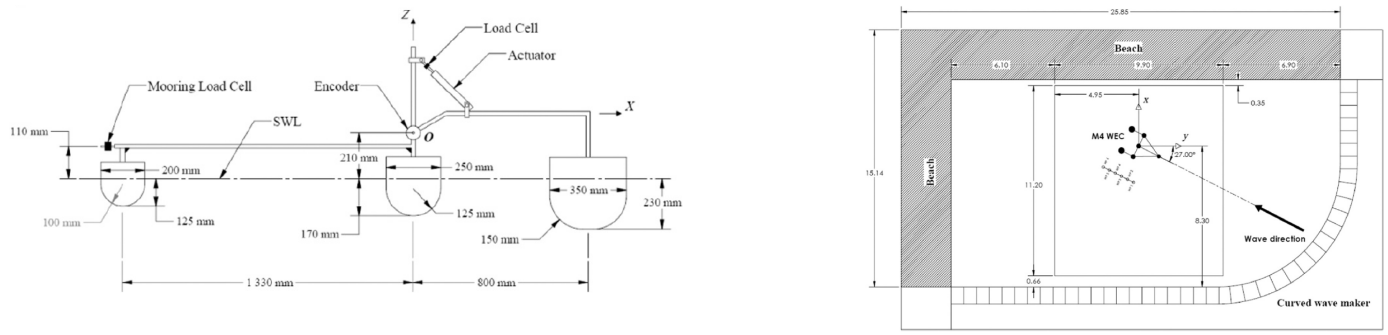

(a) (b)

Figure 15. Experimental setup used by Moreno et al., reprinted with permission from Ref. [47], 2019, Moreno et al.: (**a**) six-floater M4 WEC model with dimensions; (**b**) Lir's Ocean Basin WEC array layout.

The bow and mid floaters were rigidly connected by a beam, effectively forming a single body, and a beam from the stern floater was connected to the hinge point above the mid floater to work as PTO. The PTO damping coefficient was not controlled. Figure 15b shows the layout of the experimental setup in the Lir's Ocean Basin [47]. Stansby et al. used the six-floater M4 configuration with two PTOs to assess the results of the time-domain linear diffraction model for surge, pitch and heave floater motions in long-crested waves for multifloater configurations [52]. The angular motion at the PTOs and mooring forces were measured during different power absorptions tests. Irregular long-crested waves with JONSWAP spectra and irregular short-crested waves were applied. A test without PTO to give a worst-case response were performed as well [47].

2.11. Floating Offshore Platform with 12 WECs

The last two experimental campaigns discussed consider the integration of point-absorber WECs in a floating platform for offshore wind turbines. These technologies are in line with a recent trend to develop hybrid/synergy solutions for renewable offshore energy applications. Kamarlouei et al. studied experimentally 12 WECs concentrically arranged and attached on a floating offshore platform model [53]. Figure 16a shows the conceptual design rendering.

The 1:27 scale model was designed, built and tested in two main situations, without and with 12 cone-shaped WECs. Figure 16c shows a picture of the scale model. Besides the potential power output of the WECs, it was meant to obtain interaction between the WEC buoys and the platform to reduce the heave and pitch motions of the platform. The test was performed in the Lir NOTF medium size ocean basin at the MaREI centre of UCC, Ireland. The basin is 25 m by 17 m and 1 m deep with a moveable floor, which increases the depth up to 2.5m [53].

A wind turbine mast and nozzle were installed as a central column on the deck, thus the heeling moment caused by the weight of the wind turbine was fairly represented. The hexagonal steel frame used as the deck of the platform included connections for 12 point-absorber WECs via aluminium arms. Moreover, a set of 12 rotational friction dampers were installed in the hinge connection of the arm to the hexagonal deck. Figure 16b shows the model installation in the wave basin in detail. The model was set in the middle of the basin with a catenary mooring system with three lines. Experiments were performed for regular and irregular long-crested waves. The regular waves were simulated with 0.01, 0.02 and 0.04 m wave heights and various wave periods from 0.6 to 4.0 s. The irregular waves were simulated in seven different sea states. The floating platform was tested with and without WECs. For the former, tests were executed with and without the dampers [53].

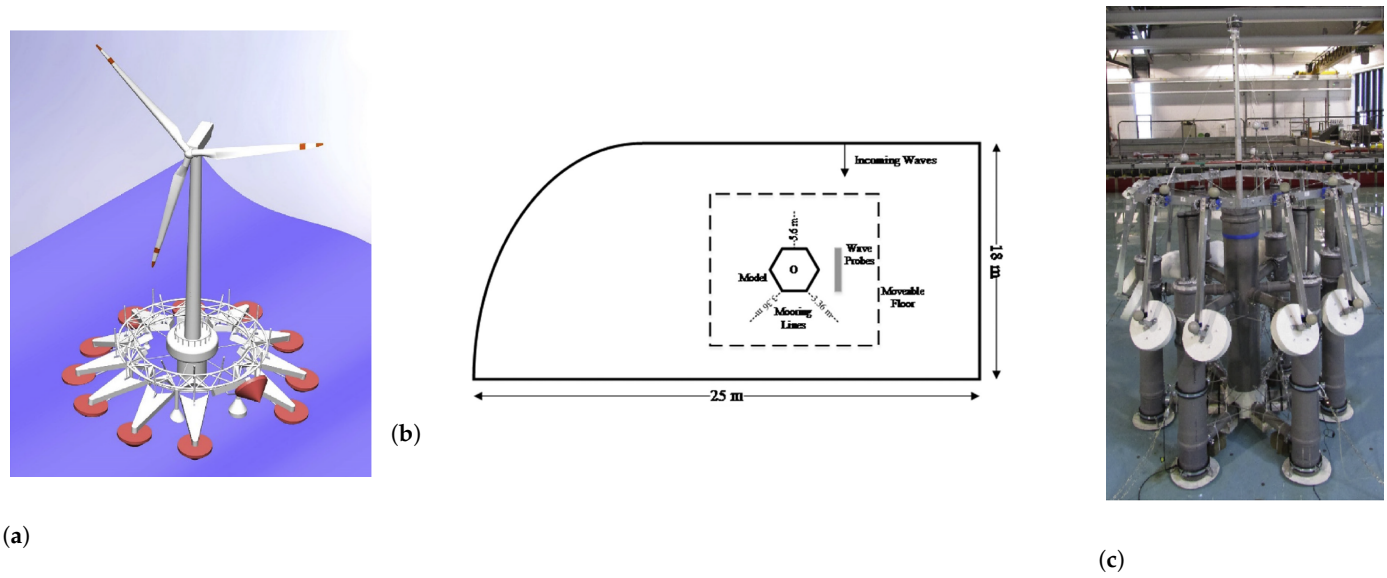

(**a**) (**b**) (**c**)

Figure 16. Experimental setup used by Kamarlouei et al., reprinted with permission from Ref. [53], 2020, Kamarlouei et al.: (**a**) conceptual design; (**b**) Lir's Ocean Basin WEC array layout; (**c**) model of the concentric WEC array installed on a floating offshore platform.

2.12. Three-Pontoon Semisubmersible Platform with Six WECs

Sun et al. performed experiments with a three-pontoon semisubmersible platform with six point-absorber WECs [54]. The platform was constructed on a 1:40 scale with a simplified hydraulic PTO system and a mooring system to restrict the platform movement. The prototype of the semisubmersible platform was WindFloat [55]. Tests were conducted in the towing tank of the National Ocean Technology Center, Tianjin, China. The towing tank is 130 m by 18 m and a water depth of 4.5 m was used. The study aimed to clarify

the interaction between the floating platform and the WEC array, without taking the influence of the wind turbine into account. The effect of the floating platform on the energy conversion of the WECs and the effect of the WECs on the hydrodynamic performance of the platform were investigated [54].

Figure 17a shows a 3D rendering of the cone bottom floater with dimensions. The PTO system is mainly made up of two hydraulic accumulators and an energy storage cylinder. Figure 17b shows the three different wave headings, their mooring system and floaters placement considered in the tests. Since the hydrodynamic performance of the floaters is different for changing wave direction, these floaters are numbered. Figure 17c shows the platform consisting of three pontoons with damping plates.

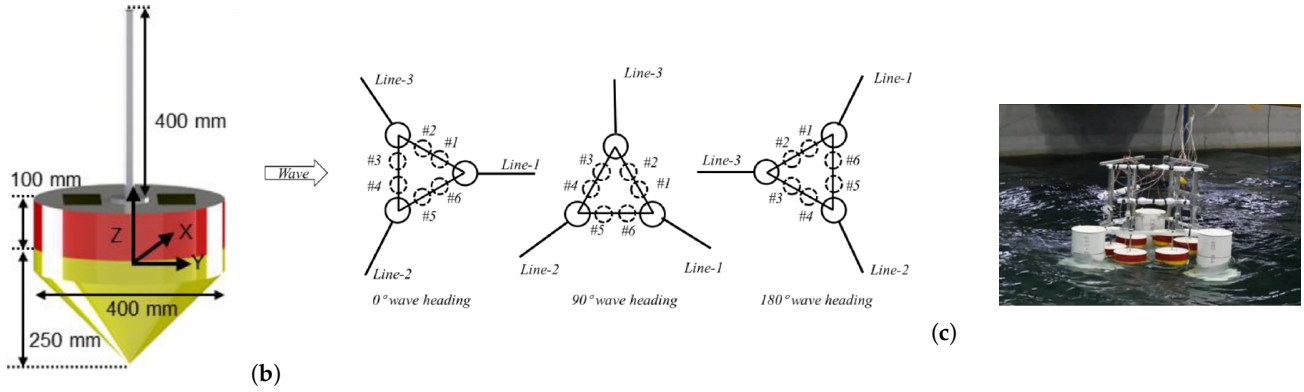

Figure 17. Experimental setup used by Sun et al., reprinted with permission from Ref. [54], 2021, Sun et al.: (**a**) 3D model of the WEC buoy with dimensions; (**b**) towing tank WEC array layout; (**c**) National Ocean Technology Center's towing tank setup.

Six floaters were fixed on the upper beam, whereas every two floaters were evenly arranged between every two pontoons. The platform's motion was measured by a six-DOF measurement system. Regular waves with wave height of 0.08 m and period of 1.0–2.2 s and irregular long-crested waves with significant wave height of 0.0975 m and peak period of 1.5 s were tested. The heave, pitch and surge response amplitude operator (RAO) of the platform were presented, for tests with and without the WECs. The RAO was defined by the ratio of the heave amplitude z and the wave amplitude η. The hydraulic power output for each of the six WECs was presented for the configurations displayed in Figure 17b [54].

3. Research Gaps

3.1. Wec Shape

Based on the literature review presented in Section 2, research gaps, knowledge gaps and opportunities within experimental modelling of point-absorber WEC arrays can be identified. Table 1 gives an overview of the point-absorber WEC array experimental campaigns available in the literature, as discussed in Section 2. For each experimental campaign, labelled with a campaign ID, the authors, year, wave testing facility and DOFs for a single WEC are summarised. The identified experimental campaigns have been carried out over the last 15 years, mainly in Europe. Besides the heave DOF, some WECs have additional DOFs. Only the experimental campaigns performed by Stratigaki et al., Nadar et al., Boere et al. and Sun et al. considered a generic WEC concept [9–12,42,54]. The other campaigns considered a scaled model of a WEC concept which was targeted for a full-scale ocean deployment in a WEC array. To the knowledge of the authors, only the Hydralab IV WECwakes project database (campaign ID 9) is made publicly available [10–13]. Göteman et al. stressed the need for available real-life data for the validation of WEC array modelling and optimisation [7]. Consequently, there is a research gap of publicly accessible experimental datasets. Preferably, a generic WEC concept should

be considered, resulting in data useful for a wide range of point-absorber WEC concepts. Tables 2–4 allow us to identify the focus and needs within these WEC array experiments.

3.2. PTO Design and Control Platform

Table 2 summarises for each experimental campaign the WEC shape, WEC diameter, PTO system and applied control strategy. Most test campaigns considered a hemisphere-cylinder for the WEC floater shape. The diameter was limited, resulting in small scale models. To limit scale effects, it is preferable to increase the WEC diameter. The WEC diameter should comply with the wave generation possibilities and dimensions of the wave testing facility, since the resonance frequency of the WEC and the WEC spacing within a WEC array depend on the diameter.

Table 1. Overview of WEC array experimental campaigns with point-absorber WECs available in the literature.

Campaign ID	Authors	Year	Wave Testing Facility	DOFs
1	Stallard et al.	2008	Wave flume, Manchester Univ.	Heave, surge
2	Thomas et al.	2008	Wave flume, Manchester Univ.	Heave, surge
3	Alexandre et al.	2009	Wave flume, Manchester Univ.	Heave, surge
4	Weller et al.	2010	Wave flume, Manchester Univ.	Heave, surge
5	Child et al.	2013	Wave basin, QUB	Heave
6	Folley et al.	2013	Wave basin, QUB	Heave
7	Lamont-Kane et al.	2013	Wave basin, QUB	Heave
8	Mackay et al.	2013	Wave basin, MARIN	6-DOF
9	Stratigaki et al.	2014	Shallow Water Basin, DHI	Heave
10	Ruiz et al.	2017	Wave basin, Aalborg University	Heave
11	Nadar et al.	2017	Wave basin, University of Tasmania	Heave, surge
12	Boere et al.	2018	Towing tank, TU Delft	Heave
13	Do et al.	2018	Wave basin, RIMS Korea	Heave, surge
14	Giassi et al.	2019	Wave basin, Univ. of Plymouth	6-DOF
15	Moreno et al.	2019	Lir wave basin, UCC	Heave, pitch, surge
16	Kamarlouei et al.	2020	Lir wave basin, UCC	Heave, pitch
17	Sun et al.	2021	Towing tank, Tianjin	Heave

It is well known that the physical design and operational quality of the PTO system used on small scale WEC models can have vast effects on the tank testing results [56]. Table 2 shows that most PTO systems are modelled as mechanical elements, such as friction brakes (campaign IDs 5, 6, 7, 9 and 16) or hydraulic dampers (campaign IDs 12, 15 and 17). These simplified PTO systems show nonlinear behaviours (e.g., static friction, temperature dependency and backlash), of which the effects propagate into the WEC power production data. The uncertainties introduced by these simplified PTO systems are seen as a major limitation for the data to be used for numerical validation and the extrapolation of the tank test results to a meaningful full ocean scale. A solution to this problem is to use actively controlled actuators for the PTO simulation by using force- (or torque)-controlled feedback systems with suitable instrumentation, enabling the PTO system to exert any desired time- and/or state-dependent reaction force [56].

Table 2 shows that most PTO systems produce a constant Coulomb damping force or resistive control, which is a simple proportional feedback with a PTO force equal to the WEC velocity times a damping factor. To implement more advanced control strategies, a highly accurate real-time controllable PTO system with bidirectional power flow is required. Test campaign 14 considered a rotational direct-driven PTO system with constant damping, showing a simple and accurate way to get a low friction PTO system with a nearly ideal velocity dependent force [8,45,46]. Only the experiments with the Manchester Bobbers (campaign IDs 1–4), the experiments with the four Wavebob WEC models (campaign ID 8),

the experiments with an array of five Wavestar WECs (campaign ID 10) and the experiments by Nadar et al. (campaign ID 11) modelled the PTO system with a motor capable of providing a bidirectional power flow (motor and generator functionality) and capable of accurately generating linear loads (force directly proportional to the velocity) [9,30–34,39,40]. Although these motors are capable of imposing advanced control strategies, advanced control was not implemented in the respective experimental campaigns. In CFD-based numerical wave tanks (CNWT), the PTO system is mostly modelled as a linear spring–damper system, not representing realistic PTO dynamics and inefficiencies and undermining the overall model fidelity [57]. To validate CNWT considering WEC arrays, it is desirable to incorporate a realistic, nonlinear PTO model. Therefore, there is a research gap of WEC array experimental data considering WECs equipped with a highly accurate real-time controllable PTO with a bidirectional power flow.

Table 2. Overview of the WEC design characteristics of the WEC array experimental campaigns of Table 1.

Campaign ID	WEC Floater Shape	WEC Diameter (m)	PTO System	Control Strategy
1	Hemisphere-cylinder	0.15	PMDC motor	Resistive control
2	Hemisphere-cylinder	0.15	PMDC motor	Resistive control
3	Hemisphere-cylinder	0.15	PMDC motor	Resistive control
4	Hemisphere-cylinder	0.15	PMDC motor	Resistive control
5	Hemisphere-cylinder	0.25	Friction brake	Coulomb damping
6	Hemisphere-cylinder	0.25	Friction brake	Coulomb damping
7	Hemisphere-cylinder	0.25	Friction brake	Coulomb damping
8	FNT with torus	0.93	Linear motor	Resistive control
9	Hemisphere-cylinder	0.315	Friction brake	Resistive control
10	Hemisphere	0.254	Linear motor	Resistive control
11	Sphere	0.25	Linear motor	Resistive control
12	Cylinder	0.25	Linear hydraulic damper	Resistive control
13	Hemisphere-cylinder	1.20	Hydraulic motor	PID velocity control
14	Ellipsoidal	0.488	Rotational direct-driven generator	Resistive control
15	Hemisphere-cylinder	0.20–0.35	Linear hydraulic damper	Resistive control
16	Cone	n.a.	Rotational friction damper	Resistive control
17	Cone	0.40	Linear hydraulic damper	Resistive control

A model predictive control (MPC) and a linear time-invariant (LTI) energy-maximising control strategy were implemented and tested for a single Wavestar WEC [56,58]. However, extending these advanced control strategies from a single WEC to an array of multiple WECs has not yet been addressed in an experimental campaign. Bacelli et al. compared two model-based WEC array control strategies, namely, global control (GC) and independent control (IC) [59]. GC is based on a centralised control algorithm which uses the complete hydrodynamic model of the WEC array whereas, with IC, each WEC is controlled independently using the hydrodynamic model of a single isolated WEC. The theoretical study suggested that a significant performance improvement (up to 10%, or more) could be obtained using GC of arrays, compared to IC [59]. Similar to the requirement of realistic PTO models within the CNWT, the incorporation of advanced control strategies into the WEC model is desirable. The nonlinear hydrodynamic environment of the CNWT allows for a more realistic evaluation of control strategies, thereby accelerating the development and implementation of energy-maximising control for WECs [57]. Therefore, there is a research gap of WEC array experimental data considering GC and advanced control on WEC array level.

3.3. Wave Conditions

Table 3 summarises for each experimental campaign the tested wave conditions. Most experimental campaigns considered both regular and irregular long-crested waves with a range of different (significant) wave heights and (peak) wave periods. In this case, the table does not make a distinction between the wave height and wave period for the regular waves and the significant wave height and peak wave period for the irregular waves, as the main purpose is to indicate the order of magnitude of the tested wave conditions.

Table 3. Overview of the tested wave conditions of the WEC array experimental campaigns of Table 1.

Campaign ID	Wave Conditions	(Significant) Wave Height (m)	(Peak) Wave Period (s)
1	Regular	0.026	0.50–1.55
2	Regular	0.026	0.57–1.33
3	Irregular (Bretschneider spectrum)	0.040	1.31
4	Regular and irregular long-crested	0.015–0.064	0.61–2.00
5	Irregular (JONSWAP spectrum)	0.025–0.038	0.89–1.26
6	Irregular short- and long-crested (JONSWAP spectrum)	0.025–0.050	0.70–1.26
7	Regular and irregular long-crested	0.014–0.075	0.67–1.26
8	Regular and irregular (JONSWAP spectrum)	0.095–0.191	1.42–2.48
9	Regular and irregular long- and short-crested	0.024–0.104	0.87–1.51
10	Regular and irregular long-crested	0.045–0.060	0.76–2.00
11	Regular	0.030–0.060	0.59–2.00
12	Regular	0.063–0.113	1.11–1.58
13	Regular	0.26	3.79
14	Regular and irregular long-crested	0.124–0.175	1.11–2.37
15	Regular and irregular long- and short-crested	0.04–0.06	0.70–2.0
16	Regular and irregular long-crested	0.010–0.139	0.60–4.0
17	Regular and irregular long-crested	0.08–0.0975	1.0–2.2

When taking the WEC diameter into account, these wave heights are mostly small, complying with the assumptions of linear potential flow theory. Only a limited number of experimental campaigns (campaign IDs 6, 9 and 15) considered irregular short-crested waves [10–12,37,47]. Focused waves are a practical laboratory method for reproducing extreme waves. From a CFD numerical modelling point of view these waves are an interesting case for validation purposes due to their peak loading and short duration time, limiting the computational cost. Therefore, there is a research gap of experimental data of WEC array tests covering extreme wave conditions, short-crested waves and focused waves, to validate recently developed nonlinear numerical models considering nonlinear effects as impact loading, friction, viscous drag, bottom slamming and vortex shedding for real sea conditions [60,61].

3.4. Number of WECs and WEC Array Layouts

Table 4 summarises for each experimental campaign the number of WECs in an array, WEC axis-to-axis separation distance, WEC array layouts, target measurements and literature references.

The number of WECs within the array ranged from 2 to 25. The axis-to-axis separation distance expressed in WEC diameters (D) ranged from 1.25 D to 20 D. The WEC array can be called closely spaced when hydrodynamic WEC–WEC interactions are significant, which also depends on the WEC floater shape besides the separation distance. The WEC array layouts tested were mainly rectilinear and staggered configurations. The target measurements to quantify near-field interactions were the absorbed power, used to calculate the capture width and the (q) interaction factor. The target measurements to quantify far-field effects were the wave field measurements. Windt et al. reported that only a few

studies modelled WEC arrays using a computational fluid dynamics (CFD) approach due to the increased computational burden when modelling WEC arrays [57]. To address the need for experimental data for the validation of CFD-based numerical models for WEC arrays, experiments should consider closely spaced WEC arrays to maximise hydrodynamic interaction. It is also preferable to increase the number of WECs in the experiments starting from two, to limit the computational cost of CNWT simulations. Therefore, there is a research gap of experimental data of WEC array tests considering a limited number of closely spaced WECs. The above-mentioned research and knowledge gaps were translated into the "WECfarm" project objectives and design requirements, summarised in Section 4.1.

Table 4. Overview of the WEC array characteristics of the WEC array experimental campaigns of Table 1.

Campaign ID	Number of WECs in an Array	Separation Distance	WEC Array Layouts	Target Measurements	Literature References
1	1, 3, 9, 12	2 D	Figure 2a	Capture width, (q) factor	[30]
2	5	2 D	Figure 2b	Heave amplitude	[31]
3	5, 10	2 D	Figure 3a	Wave field	[32]
4	12	2 D	Figure 3b	Capture width, (q) factor	[33–35]
5	22, 24	3 D	Figure 5a	Absorbed power, (q) factor	[36,62]
6	22, 24	3 D	Figure 5a	(q) factor	[37]
7	4	3 D	Figure 4b	Capture width, wave field	[38]
8	4	8.5 D	Figure 6b	Absorbed power	[39]
9	1–25	5–10–20 D	Figure 8b	(q) factor, wave field	[10–12]
10	5	5 D	Figure 9b	Absorbed power	[40,58]
11	1, 2, 4, 6	6 D; 4 D	Figure 11b	(q) factor	[9]
12	2	2 D–6 D	Figure 12b	Absorbed power	[42]
13	1, 10	>3 D	Figure 13a	q factor	[43,44]
14	6	4 D	Figure 14a	Absorbed power, (q) factor	[8,45,46]
15	3, 6, 8	2 D–7 D	Figure 15a	Absorbed power, capture width	[47]
16	12	<2 D	Figure 16b	Rotational velocity	[53]
17	6	1.25 D	Figure 17b	Absorbed power	[54]

4. Design of the WECfarm Project Setup

4.1. Research Objectives and Design Requirements

The experimental "WECfarm" project was initiated by Ghent University in 2018 targeting to deliver an experimental dataset on wave–WEC and WEC–WEC interactions for point-absorber WEC array tests. This dataset aims to cover the research gap on the need for publicly available real-life and reliable data for the validation of WEC array modelling and WEC array optimisation. The dataset will contain measurement time series at a sufficient high sample rate of the parameters fully characterising the experiments, aiming to minimise measurement uncertainties. The objective of the "WECfarm" project is to design, construct and test a point-absorber WEC array which addresses the research and knowledge gaps discussed in Section 3. Summarised, the WECfarm project objective is to address the need for WEC array tests with:

1. A generic WEC concept, resulting in data useful for a wide range of point-absorber concepts.
2. WECs equipped with a highly accurate, real-time actively controllable PTO system with bidirectional power flow.
3. A control platform to implement GC and advanced control on WEC array level.
4. A wide range of wave conditions. These should include regular waves, irregular long- and short-crested waves, focused waves and extreme wave conditions.
5. A limited number of closely spaced WECs.

Section 4.2 discusses how the "WECfarm" WEC hydrodynamic design addresses requirements 1 and 5, Section 4.3 discusses how the "WECfarm" WEC electromechanical design addresses requirement 2 and Section 4.4 discusses how the "WECfarm" WEC array DAQ and control platform addresses requirement 3. Section 4.5 discusses the methodology within the "WECfarm" project, mentioning the wave basin testing performed so far and the scheduled testing, addressing requirement 4.

4.2. Hydrodynamic Design

To simplify the physical and numerical modelling of the WEC and the WEC arrays, the DOFs for the "WECfarm" WEC were restricted to heave. Shadman et al. performed a numerical geometrical optimisation for heaving point-absorber WECs [63]. The study evaluated cylindrical buoys for different diameter-to-draft ratios based on the maximum power absorption, the natural period and the resonance bandwidth, defined as the frequency interval in which the absorbed power is more than half of its maximum value. These metrics can be derived from the RAO. The study found that cylindrical buoys with larger diameters and relatively small drafts provided a good resonance bandwidth, while the maximum energy absorption was achievable in the same diameter range with larger drafts. In general, a larger diameter improved the buoy performance by increasing the maximum power, natural period and resonance bandwidth. Increasing the draft led to a higher maximum power and natural period with a lower resonance bandwidth. Therefore, modifying the draft could significantly influence the point absorber performance. A numerical optimiser defined the best set of geometrical parameters which jointly maximised the maximum power and resonance bandwidth for the design sea state, resulting in a diameter-to-draft ratio of 4.5 [63].

Bacelli et al. designed and tested a generic six-DOFs WEC on scale of 1:17 [64]. The study found that a good point absorber was characterised by a flat response, meaning that it was able to extract power from waves without requiring reactive power from the PTO system over a broad frequency range. Therefore, a slender cylinder was not a good absorber since it had a high sensitivity of the absorbed power with respect to the wave frequency. An additional consideration was that good absorbers were also characterised by a relatively small oscillation amplitude, resulting in a smaller PTO stroke. The designed WEC buoy had a cylindrical shape with a diameter-to-draft ratio of 3.3 and a 34.9° truncation of the bottom extending over 7/10 of the draft [64].

Based on the findings and insights of Shadman et al. [63] and Bacelli et al. [64], an iterative numerical optimisation study was performed on the geometry of the "WECfarm" WEC. The scale of the "WECfarm" WEC was chosen based on a combination of the Coastal and Ocean Basin's (COB) (Ostend, Belgium) characteristics [65] and on a workable and fundable model scale. Given the available funding for the "WECfarm" project experimental setup, the complexity related to requirements 2 and 3 in Section 4.1, the number of WECs was set equal to five, complying with requirement 5 in Section 4.1. Linear potential flow simulations with WEC's axis-to-axis spacing of 2 D confirmed that this number was sufficient to obtain significant WEC–WEC interactions and to study the wave–WEC interactions for WEC arrays with two to five WECs.

To reduce the surge force loading and increase the radiation capacity to enhance near-field interactions, the WEC buoy was designed with a diameter-to-draft ratio of 3.75. The WEC buoy bottom was truncated under an angle of 45° over a height of 0.10 m. Therefore, the radius of the WEC buoy at the truncation part ranged from 0.20 m to 0.30 m. The WEC buoy was 0.32 m high and designed with a draft of 0.16 m. This draft corresponded with a submerged volume of 0.03683 m^3. Therefore, the mass of the WEC buoy and heaving parts on top of it was 36.83 kg. The angle of 3° on the cylindrical part was required for the thermoforming construction process to allow the removal of the acrylonitrile butadiene styrene (ABS)-truncated cylindrical WEC buoy from the wooden mould. Figure 18a shows a 2D rendering of the final geometry of the "WECfarm" WEC buoy with its dimensions and the adopted coordinate system. The WEC buoy is axisymmetric around the z-axis.

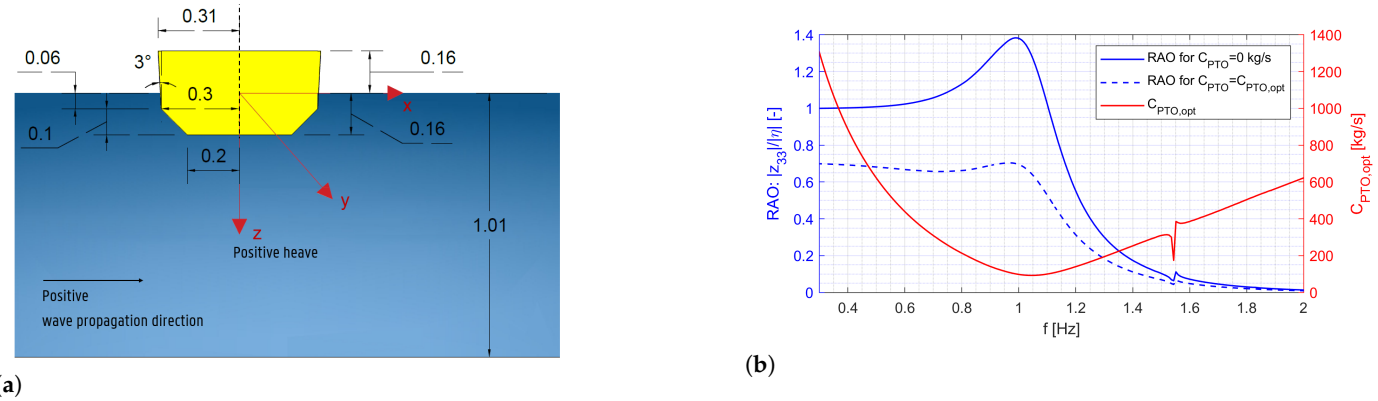

(**a**)

(**b**)

Figure 18. WECfarm's WEC's buoy: (**a**) 2D rendering with dimensions in m; (**b**) RAO and $C_{PTO,opt}$.

Figure 18b shows the RAO for the free response case, equivalent to a PTO damping of 0 kg/s and the RAO for the case with the optimal PTO damping for the resistive control strategy, $C_{PTO,opt}$, according to:

$$C_{PTO,opt}(\omega) = \sqrt{B^2(\omega) + \left(\omega(M + A(\omega)) - \frac{\rho g S}{\omega}\right)^2} \quad (2)$$

in which $B(\omega)$ corresponds to the hydrodynamic damping and $A(\omega)$ to the added mass [66]. The mass (M) was equal to 36.83 kg, ρ is the water density equal to 1000 kg/m^3, (g) is the gravitational acceleration of 9.81 m/s^2 and S is the cross-sectional area of the buoy at the unperturbed SWL. Figure 18b also displays $C_{PTO,opt}$. The heave wave excitation coefficients, $B(\omega)$ and $A(\omega)$ were obtained with the open-source software package openWEC [67], with the integration of the BEM code Nemoh. As recommended by Shadman et al. [63] and Bacelli et al. [64], the RAO had a flat response, resulting in a high resonance bandwidth. The numerically obtained natural period was slightly higher than 1.0 s. This relatively small natural period had the advantage to avoid a sharp power absorption decrease for lower wave periods, since the WEC buoy was designed with dimensions to operate in wave conditions with higher wave periods.

Since the "WECfarm" project targets experimental data necessary for the validation of nonlinear numerical models for WEC arrays, viscous drag effects are important [61]. Moreover, the limited draft in combination with the flat bottom will result in important bottom slamming effects for tests where the WEC buoy re-enters the water after being lifted out [60].

4.3. Electromechanical Design

Figure 19 shows a 3D rendering of the final design of the "WECfarm" WEC. The used right-handed coordinate system has its origin at the intersection of the still water level (SWL) with the vertical axis through the centre of the WEC buoy. This allows one to express displacements of the WEC buoy relative to the SWL. The x-axis corresponds with the positive wave propagation direction. The y-axis follows from the motor sign convention: a positive torque results in a downward motion of the WEC buoy. Therefore, the z-axis is pointed downwards to define positive forces, displacements, velocities and accelerations. Figure 19 also indicates the three translations, surge (1), sway (2) and heave (3), and the three rotations, roll (4), pitch (5) and yaw (6).

To exclude friction in the linear guiding, air bushings were used. The surge excitation force, acting in the centre of buoyancy, results in a moment on the linear guiding system. This moment can be decoupled in normal forces by a configuration of three air bushings. The air bushings are characterised by a load versus pressure curve, where one 40 mm OAV (OAV Air Bearings, Princeton, NJ, USA) air bushing can cope with a maximum radial load of 720 N, for a nominal pressure of 5.5 bar [68]. A configuration of three OAV 40 mm air bushings guarantees a permanent layer of air between the guide shafts and the bushings for

the most extreme wave conditions, resulting in zero-friction linear guiding on the condition of a proper alignment. The air bushings coefficient of friction is a function of air shear from motion, not from surface contact. Therefore, at zero velocity, there would be zero friction and making infinite motion resolution theoretically possible. A friction coefficient of 0.00008 in log-scale due to the contribution from air molecules and gravitation can be taken into account [68]. To obtain this air gap, a compressor with a two-stage air filter supplies these bushings with clean and dry air under a nominal pressure of 5.5 bar. The OAV 40 mm air bushings require a shaft's outside diameter of 40.00 mm +0.00/−0.02 mm (tolerance class g6). Therefore, MiSUMi (MiSUMi Europe, Frankfurt am Main, Germany) shafts with tolerance class g6 were custom configured.

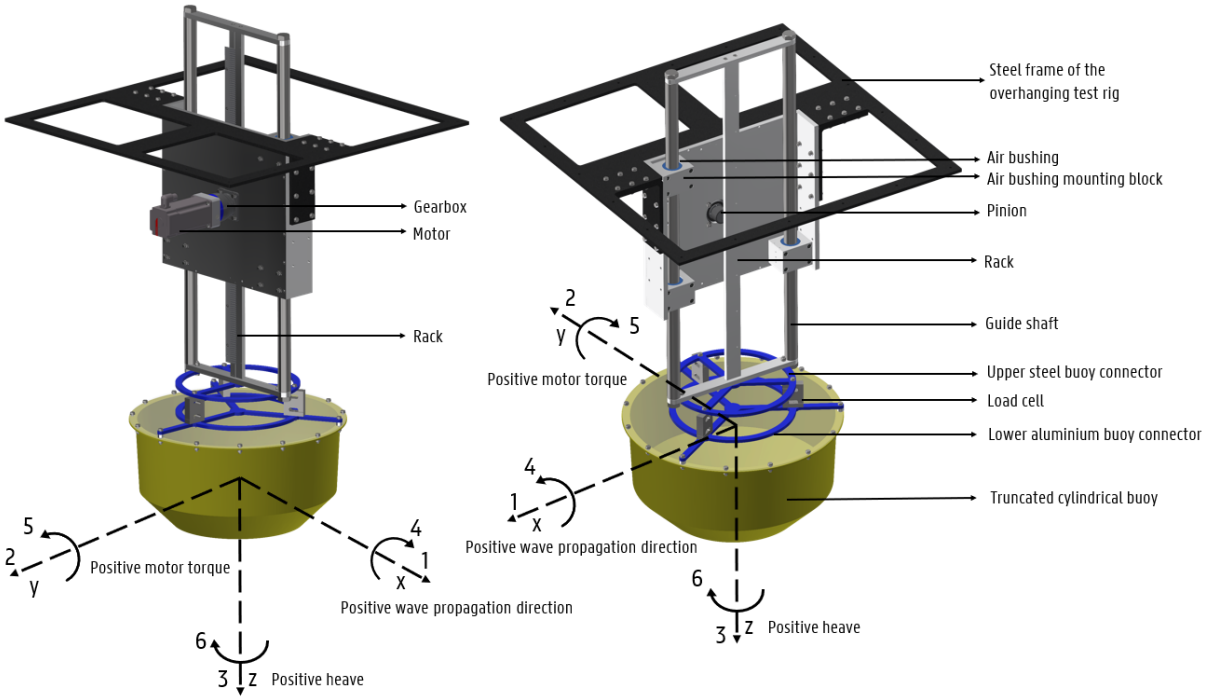

Figure 19. Rendering of the "WECfarm" WEC, made with Autodesk Inventor (Autodesk, San Rafael, CA, USA).

The WEC was mounted on a steel frame structure, designed to be rigid enough to avoid resonance at low frequencies. The total structure was designed for flexible (dis)assembly and installation in any facility. The steel frame was provided with M8 connection holes to allow mounting on MiniTec (MiniTec, Schönenberg-Kübelberg, Germany) profiles, or equivalent. This frame can be flipped 180° to install the WEC on the side walls of a wave flume or water basin.

The PTO system of the WEC was designed as a permanent magnet synchronous motor (PMSM) connected to a gearbox powering a rack and pinion system. A gearbox can offer a solution to deal with high forces at low velocities in wave energy applications. Bacelli et al. described that the Coulomb friction in the drivetrain attributed to the gearbox significantly degraded the quality of open-loop force control, necessitating the use of closed-loop control [59]. Therefore, a single-stage low-ratio transmission was desired. A Wittenstein (Wittenstein, Igersheim, Germany) single-stage gearbox "NPR 025S-MF1-4-2E1-1S" with a ratio i = 1:4 connects the pinion with the motor. The gearbox has a slotted-hole connection, allowing to slide the pinion in the rack to minimise backlash in the transmission. The pinion has 20 teeth and a pitch circle radius R_{pinion} of 0.0212205 m. Given the pinion helix angle of 19.5283°, the backlash can be at a maximum +−0.3 mm. The velocity on the pinion will be four times less than on the motor shaft, while the torque on the pinion will be four times more than on the motor shaft.

A PMSM was chosen since it can provide the bidirectional power flow necessary for reactive control, high-bandwidth open-loop force control and high-accuracy control and feedback (position, velocity and torque). The motor's torque–speed curves for a range of target test wave conditions (regular and irregular long-crested) were calculated with a MATLAB Simscape electromechanical system model coupled with the open-source code WEC-Sim for simulating WECs. This design procedure resulted in the selection of a Beckhoff (Beckhoff Automation, Verl, Germany) PMSM "AM8041-2D11-0000" with an inertia of 1.73 kg cm^2, a rated torque of 2.33 Nm and a rated speed of 1500 RPM, for a 230 V AC power supply [69]. The motor is equipped with a holding brake, mechanically operated by a solenoid, to make it possible to keep the WEC buoy lifted out of the water. When the motor is not operational, the mechanical brake is activated. The Beckhoff PMSM is powered and controlled by a Beckhoff motor drive. For the setup of five WECs, two Beckhoff motor drives type "AX5203-0000-0213" power each two motors and a third Beckhoff motor drive type "AX5103-0000-0212" powers the fifth WEC. The three drives will be daisy-chained with EtherCAT cables. The drive consumes the power generated by the WECs in the intermediate circuit. Therefore, no ballast resistor is needed.

4.4. DAQ and Control Platform for the Five-WEC Array

Figure 20 shows a scheme of the data acquisition and control flow for the "WECfarm" setup with five WECs, with a legend indicating the signal type. The MATLAB-Simulink real-time control model was built on the host PC and loaded on the Speedgoat (Speedgoat, Köniz, Switzerland) Performance real-time target machine via Ethernet communication. This target machine ran the Simulink model and processed the input/output (I/O) at a sample frequency of 1000 Hz. In this context, the high sample frequency corresponded with the defined "real-time" terminology. The target screen displayed diagnostic info of the execution process steps of the Simulink model. The sensor input for the Speedgoat target machine was realized with a Speedgoat IO133-Performance analogue and digital I/O module, which is a fast, simultaneous-sampling, 16-bit analogue input and output module with Simulink driver blocks. A scheme on the bottom of Figure 20 shows the sensor input for the Speedgoat IO133 terminal board for each of the five WECs. The accelerometer ADXL335 (Analog Devices, Norwood, MA, USA) was used to measure the acceleration of the WEC buoy in the heave direction and was attached on top of the rack, the furthest position on the WEC from the water. Three Althen (Althen Sensors & Controls BV, Rijswijk, The Netherlands) FLH3 50 kg load cells were placed between the hydrodynamic part (the buoy) and the electromechanical part (the motor) to measure the actual applied forces. These three load cells allowed the possibility to close the loop around the force. However, Bacelli et al. stressed that closing the loop around a force sensor may induce negative consequences for the design of higher-level control loops [59]. A configuration of at least three load cells was required to avoid torsion and bending influencing the measurements. A TLE analogue weight transmitter (Laumas Elettronica, Montechiarugolo, Italy) was used to amplify these three analogue signals and to sum them to one analogue signal. In case the WEC is locked, the wave heave excitation force can be measured. In case the motor is active, the load cells measure the PTO force. The upper microswitch and the lower microswitch were used as safety limit switches. It is necessary to limit the amplitude of the WEC buoy displacement to prevent the guiding system damaging the structure. The laser sensor Micro-Epsilon optoNCDT 1420 (Micro-Epsilon, Ortenburg, Germany) was installed on one WEC as a backup for the motor encoder to measure the displacement of the WEC buoy relative to the SWL. Moreover, the laser sensor could be used for displacement measurements for tests without a motor.

The torque request in the Simulink model is sent by the EtherCAT (Ethernet for Control Automation Technology) communication protocol to the Beckhoff motor drive as a master data telegram (MDT) process parameter. On the other hand, the Speedgoat target machine can receive by EtherCAT communication amplifier telegram (AT) process parameters from the Beckhoff motor drive. Normally, a Beckhoff motor drive is controlled by a Beckhoff's

industrial PC, serving as a programmable logic controller (PLC). For the WECfarm project, it was decided to configure the Speedgoat target machine as a master and the Beckhoff drive as a slave. This allowed us to benefit from the control and postprocessing possibilities within the MATLAB-Simulink environment. To establish the communication between the Speedgoat target and the Beckhoff drive, the EtherCAT network needs to be initialised in the Simulink model with the EtherCAT initialisation block. This block requires to load an EtherCAT network information (ENI) file containing the motor topology and process parameters. To create this ENI file, a Beckhoff industrial PC was used. When this Beckhoff industrial PC is connected by an EtherCAT cable to the Beckhoff drive with motor, Beckhoff TwinCAT 3 software can scan the network to define the motor topology. The user can configure the operation modes and select the required MDT and AT process parameters. Consequently, the result of this process can be exported as an .xml ENI file to initialise the EtherCAT network in the Simulink model. On their turn, the Beckhoff PMSM input and output signals are processed by the Beckhoff motor drive by the "One Cable Technology", allowing to send commands and feedback using the same cable. The drive receives the 18-bit resolution position values from the single-turn absolute encoder. This encoder allows the real-time determination of the state (position and velocity) of the WEC buoy. The drive provides the motor with a certain current, corresponding with a torque multiplication with the torque constant of 1.43 Nm/A.

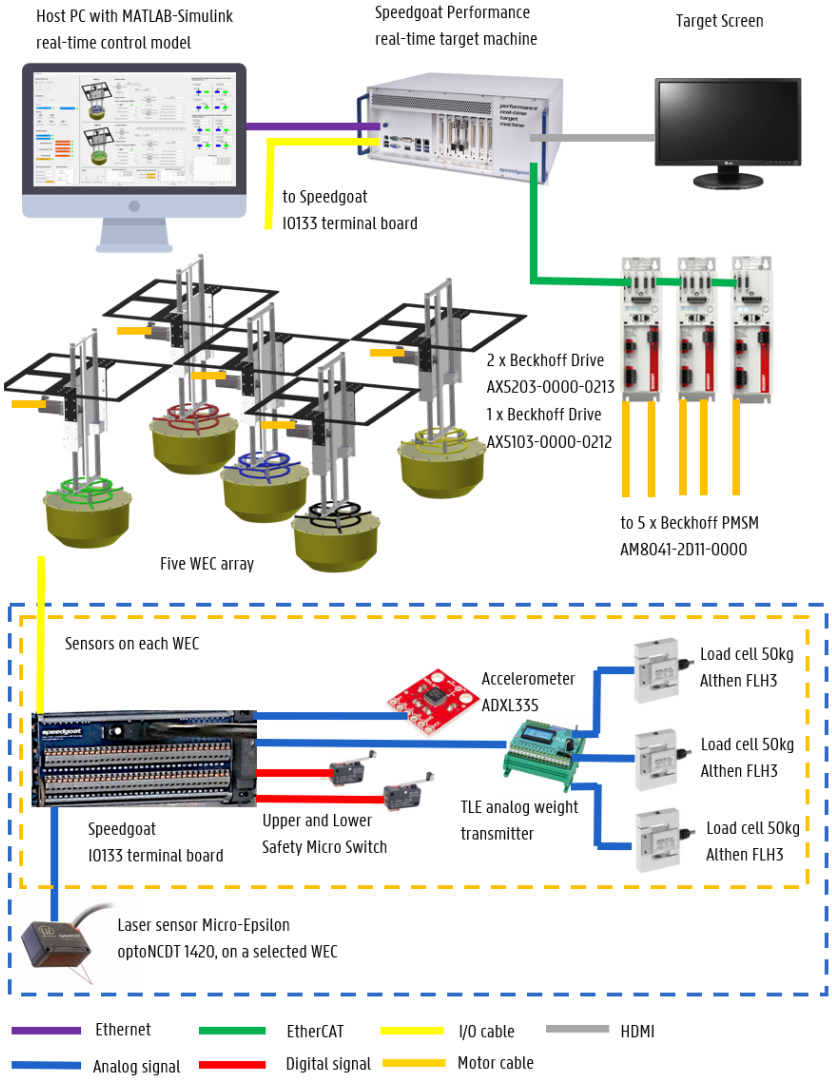

Figure 20. General data acquisition and control flow for the "WECfarm" five-WEC array.

4.5. The "WECfarm" WEC Array Approach

To obtain the experimental dataset on point-absorber WEC array tests, the "WECfarm" project consisted of the following consecutive steps, involving a gradual increase in complexity. In 2019, the "WECfarm" WEC was designed and numerically modelled. In 2020–2021, the first "WECfarm" WEC was constructed and tested in a small water basin (see Figure 21a) at the Coastal Engineering Research Group of Ghent University (Belgium) to evaluate all structural, mechanical, electronic, data acquisition and control aspects before deploying the WEC in a wave basin to evaluate the hydrodynamic performance.

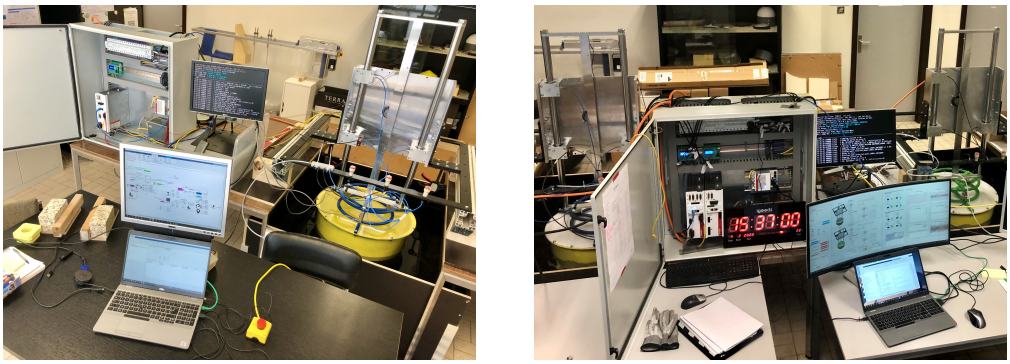

(**a**) (**b**)

Figure 21. "WECfarm" experimental setup at the Coastal Engineering Research Group of Ghent University (Belgium): (**a**) single WEC; (**b**) two WEC array.

In April 2021, this first "WECfarm" WEC was tested in the wave basin of Aalborg University (Denmark). Figure 22a shows a picture of the experimental setup. The hydrodynamical performance was assessed by the execution of system identification (SID) tests (radiation, excitation and free decay tests). The passive, reactive and latching controller were tested for a selection of regular and irregular long-crested waves.

In late 2021, an array of two "WECfarm" WECs was constructed and tested in two small water basins (see Figure 21b) at the Coastal Engineering Research Group of Ghent University (Belgium) to test the two-WEC array Simulink control model prior to wave basin testing.

In February 2022, an array of two "WECfarm" WECs was tested in the wave basin of Aalborg University (Denmark) to quantify wave–WEC and WEC–WEC interactions. Figure 22b shows a picture of the experimental setup. The WECs were placed in a row layout, with an axis-to-axis separation distance equal to 1.20 m, equivalent to 2 D. Based on SID radiation tests, causal impedance matching proportional (P) and proportional–integral (PI) controllers were designed [70,71]. These controllers, corresponding to resistive and reactive control, respectively, were tested for a selection of irregular long-crested waves. It should be mentioned that in the test campaign with a singe WEC, a Beckhoff PMSM "AM8542-2E11-0000" with an inertia of 6.17 kg cm^2 was used, updated to a Beckhoff PMSM "AM8041-2D11-0000" with an inertia of 1.73 kg cm^2 in the test campaign with the two-WEC array [69]. Theoretically, maximum accuracy with maximum dynamics can be reached when the ratio of system inertia to motor inertia is one. The motor for the first test campaign was designed to have this ratio lower than two, which was increased to ten based on the evaluation of the dynamics after the first test campaign. This lower motor inertia resulted in a higher natural frequency of the WEC.

Experimental testing of arrays of up to five "WECfarm" WECs is planned in 2023, in the new wave basin, the COB in Ostend (Belgium) [65]. This planned test campaign will deliver the main publicly available dataset for wave–WEC and WEC–WEC interactions. Moreover, the "WECfarm" WEC array experimental setup is meant to serve as a test-bed for future research, to deal with challenges defined within requirement 3 in Section 4.1.

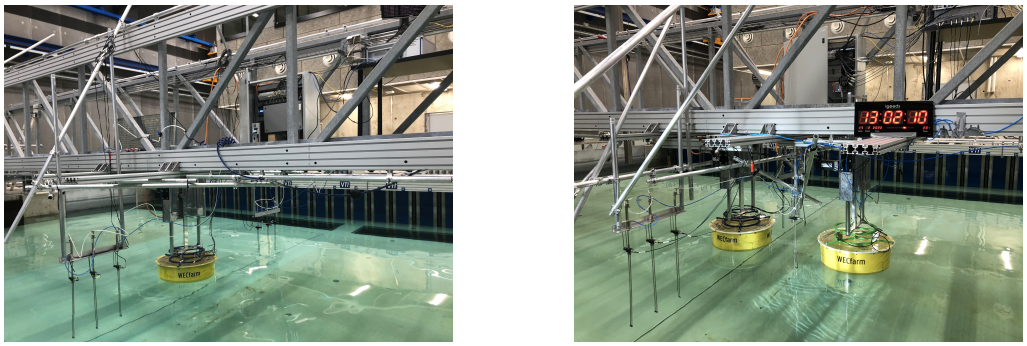

(a) (b)

Figure 22. "WECfarm" experimental setup at the Aalborg University wave basin:(**a**) single WEC (April 2021); (**b**) two WEC array (February 2022).

5. Discussion and Conclusions

Experimental wave basin testing with arrays of two to five heaving point-absorber WECs within the "WECfarm" project aims to address the need for publicly available real-life data for the validation of WEC array numerical modelling and optimisation by establishing a dataset for the research community. This article provided a comprehensive literature review on experimental modelling of point-absorber WEC arrays, which allowed us to identify research gaps, to be addressed in the "WECfarm" project. These research gaps were reformulated as design requirements for the "WECfarm" experimental setup.

The designed truncated cylindrical "WECfarm" WEC buoy addressed the need for WEC array tests with a generic WEC concept on a suitable scale, resulting in data useful for a wide range of point-absorber concepts. The hydrodynamic design was optimised to enhance near-field interactions, based on literature findings and linear potential flow numerical simulations. The truncated cylindrical buoy had a draft of 0.16 m and a radius of 0.30 m. The mass of the hydrodynamic activated part was 36.83 kg. The RAO showed a resonance peak around 1.0 s. The high diameter-to-draft ratio of 3.75 resulted in a flat RAO response and high resonance bandwidth. A limited number of five closely spaced WECs was fundable and confirmed to be sufficient to study near-field interactions based on linear potential flow numerical simulations.

The WECs were equipped with a PMSM, addressing the need for WEC array tests with a highly accurate, real-time actively controllable PTO system with bidirectional power flow. The EtherCAT communication protocol allowed us to send motor commands and receive motor feedback at high resolution and sample rate, enabling advanced WEC control. This PTO system will overcome the shortcoming of uncertainties introduced by simplified PTO systems (e.g., friction brakes and hydraulic dampers) used within previously performed WEC array experimental campaigns. Moreover, the "WECfarm" WEC was designed with an air bushings linear guiding system to exclude guiding friction in the power absorption measurements.

The control with a Speedgoat Performance real-time target machine offers the possibility to implement GC and advanced WEC array control strategies in the MATLAB-Simulink model and test accordingly. This centralised control platform overcomes the limitation of former WEC array experimental setups where control could only be implemented at the level of individual WECs. Besides the motor feedback to determine the WEC position and velocity, each WEC was equipped with an accelerometer and a configuration of three load cells, providing accurate measurements.

Wave basin testing within the "WECfarm" project will cover a wide range of wave conditions, including regular waves, irregular long- and short-crested waves, focused waves and extreme wave conditions. This overcomes the shortcoming of previously performed WEC array experimental campaigns only considering small amplitude regular and irregular long-crested waves, and not meeting the current requirements to validate CNWTs with WEC arrays.

Within the "WECfarm" project, two test campaigns were performed at the Aalborg University wave basin: (a) a testing of the first WEC in April 2021 and (b) a testing of a two-WEC array in February 2022. An experimental campaign with arrays of up to five "WECfarm" WECs is planned in the COB in Ostend (Belgium) in 2023. The dataset of each test campaign will be made available to the research community for numerical model validation and WEC array optimisation purposes.

Author Contributions: Conceptualisation, methodology and analysis, T.V.; writing—original draft preparation, T.V.; electromechanical design of the WECfarm's WEC: T.V., B.D.B. and K.S.; writing—review and editing, V.S., M.V. and P.T.; funding acquisition for the WECfarm's experimental setup, V.S. and P.T. All authors have read and agreed to the published version of the manuscript.

Funding: This work is supported by the FWO (Fonds Wetenschappelijk Onderzoek - Research Foundation Flanders), Belgium, through the following funding: (1) Timothy Vervaet is a Ph.D. fellow (fellowship 11A6919N); (2) Vasiliki Stratigaki is a postdoctoral researcher (fellowship 1267321N) and has been granted the "FWO Research Grant" for constructing the WEC experimental setup (FWO-KAN-DPA376).

Institutional Review Board Statement: Not applicable.

Informed Consent Statement: Not applicable.

Data Availability Statement: The datasets resulting from the WECfarm project will be made available in due time at https://www.awww.ugent.be, accessed on 29 May 2022.

Acknowledgments: OAV (https://www.oavco.com/, accessed on 29 May 2022) is acknowledged for providing educational discount on the OAV 40 mm air bushings used in the experimental setup as well as for providing technical support [68]. Beckhoff, Wittenstein and Speedgoat are acknowledged for providing technical support.

Conflicts of Interest: The authors declare no conflict of interest. The funders had no role in the design of the study; in the collection, analyses, or interpretation of data; in the writing of the manuscript, or in the decision to publish the results.

Abbreviations

The following abbreviations are used in this manuscript:

ABS	Acrylonitrile butadiene styrene
AT	Amplifier telegram
BEM	Boundary element method
CFD	Computational fluid dynamics
CNWT	CFD-based numerical wave tank
COB	Coastal and Ocean Basin
DAQ	Data acquisition system
DOFs	Degrees of freedom
ENI	EtherCAT network information
EtherCAT	Ethernet for Control Automation Technology
FNT	Float-neck-tank
GC	Global control
IC	Independent control
I/O	Input and output
JONSWAP	Joint North Sea Wave Project
LTI	Linear time-invariant
MDT	Master data telegram
MPAWEC	Multipoint-absorber wave energy converter
MPC	Model predictive control
MWL	Mean water level
OWC	Oscillating water column
P	Proportional
PerAWaT	Performance Assessment of Wave and Tidal array systems

PI	Proportional–integral
PID	Proportional–integral–derivative
PLC	Programmable logic controller
PMDC	Permanent magnet direct current
PMSM	Permanent magnet synchronous motor
PTFE	Polytetrafluoroethylene
PTO	Power take-off
QUB	Queen's University Belfast
RAO	Response amplitude operator
RIMS	Research Institute of Small and Medium Shipbuilding
SID	System identification
SWL	Still water level
UCC	University College Cork
WEC	Wave energy converter

References

1. Falnes, J.; Lillebekken, P.M. Budal's latching-controlled-buoy type wave-power plant. In Proceedings of the 5th European Wave Energy Conference, Cork, Ireland, 17–20 September 2003; pp. 233–244.
2. Yang, S.H.; Ringsberg, J.W.; Johnson, E. Wave energy converters in array configurations—Influence of interaction effects on the power performance and fatigue of mooring lines. *Ocean. Eng.* **2020**, *211*, 107294. [CrossRef]
3. Budal, K. Theory for absorption of wave power by a system of interacting bodies. *J. Ship Res.* **1977**, *21*, 248–253. [CrossRef]
4. Xie, J.; Zuo, L. *Dynamics and Control of Ocean Wave Energy Converters*; Mechanical Engineering Department, State University of New York: Stony Brook, NY, USA, 2013.
5. Coe, R.G.; Bacelli, G.; Wilson, D.G.; Abdelkhalik, O.; Korde, U.A.; Robinett, R.D. A comparison of control strategies for wave energy converterss. *Int. J. Mar. Energy* **2017**, *20*, 45–63. [CrossRef]
6. Garcia-Rosa, P.B.; Bacelli, G.; Ringwood, J.V. Control-Informed Optimal Array Layout for Wave Farms. *IEEE Trans. Sustain. Energy* **2011**, *6*, 575–582. [CrossRef]
7. Göteman, M.; Giassi, M.; Engström, J.; Isberg, J. Advances and Challenges in Wave Energy Park Optimization—A Review. *Front. Energy Res.* **2020**, *8*, 26. [CrossRef]
8. Giassi, M.; Thomas, S.; Shahroozi, Z.; Engström, J.; Isberg, J.; Tosdevin, T.; Hann, M.; Göteman, M. Preliminary results from a scaled test of arrays of point-absorbers with 6 DOF. In Proceedings of the 13th EuropeanWave and Tidal Conference (EWTEC), Napoli, Italy, 1–6 September 2019.
9. Nader, J.R.; Fleming, A.; Macfarlane, G.; Penesis, I.; Manasseh, R. Novel experimental modelling of the hydrodynamic interactions of arrays of wave energy converters. *Int. J. Mar. Energy* **2017**, *20*, 109–124. [CrossRef]
10. Stratigaki, V.; Troch, P.; Stallard, T.; Forehand, D.; Kofoed, J.P.; Folley, M.; Benoit, M.; Babarit, A.; Kirkegaard, J. Wave basin experiments with large wave energy converter arrays to study interactions between the converters and effects on other users in the sea and the coastal area. *Energies* **2014**, *7*, 701–734. [CrossRef]
11. Stratigaki, V.; Troch, P.; Stallard, T.; Forehand, D.; Folley, M.; Kofoed, J.P.; Benoit, M.; Babarit, A.; Vantorre, M.; Kirkegaard, J. Sea-state modification and heaving float interaction factors from physical modelling of arrays of wave energy converters. *J. Renew. Sustain. Energy* **2015**, *7*, 061705. [CrossRef]
12. Stratigaki, V. Experimental Study and Numerical Modelling of Intra-Array Interactions and Extra-Array effects of Wave Energy Converter Arrays. Ph.D. Thesis, Ghent University, Faculty of Engineering and Architecture, Ghent, Belgium, 2014.
13. WECwakes. Large Scale Experiments on Wave Energy Converter Farms to Study the Near-Field Effects between the Converters and the Far-Field Effects on Other Users in the Coastal Area. 2014. Available online: https://hydralab.eu/research--results/ta-projects/project/16/ (accessed on 20 May 2022).
14. Balitsky, P.; Verao Fernandez, G.; Stratigaki, V.; Troch, P. Assessment of the power output of a two array clustered WEC farm using a BEM solver coupling and a wave propagation model. *Energies* **2018**, *11*, 2907. [CrossRef]
15. Devolder, B.; Stratigaki, V.; Troch, P.; Rauwoens, P. CFD simulations of floating point absorber wave energy converter arrays subjected to regular waves. *Energies* **2018**, *11*, 641. [CrossRef]
16. Verao Fernandez, G.; Stratigaki, V.; Troch, P. Irregular wave validation of a coupling methodology for numerical modelling of near and far field effects of wave energy converter arrays. *Energies* **2019**, *12*, 538. [CrossRef]
17. Verbrugghe, T.; Stratigaki, V.; Altomare, C.; Domínguez, J.; Troch, P.; Kortenhaus, A. Implementation of open boundaries within a two way coupled SPH model to simulate nonlinear wave structure interactions. *Energies* **2019**, *12*, 697. [CrossRef]
18. Sheng, W.; Tapoglou, E.; Ma, X.; Taylor, C.J.; Dorrell, R.M.; Parsons, D.R.; Aggidis, G. Hydrodynamic studies of floating structures: Comparison of wave-structure interaction modelling. *Ocean. Eng.* **2022**, *249*, 110878. [CrossRef]
19. Sheng, W.; Tapoglou, E.; Ma, X.; Taylor, C.J.; Dorrell, R.M.; Parsons, D.R.; Aggidis, G. Time-Domain Implementation and Analyses of Multi-Motion Modes of Floating Structures. *J. Mar. Sci. Eng.* **2022**, *10*, 662. [CrossRef]
20. Falnes, J. *Ocean Waves and Oscillating systems: Linear Interactions Including Wave-Energy Extraction*; Cambridge University Press: Cambridge, UK, 2004.

21. Falnes, J.; Hals, J. Heaving buoys, point absorbers and arrays. *Philos. Trans. Math. Phys. Eng. Sci.* **2012**, *370*, 246–277. [CrossRef]
22. Sheng, W.; Alcorn, R.; Lewis, T. Physical modelling of wave energy converters. *Ocean. Eng.* **2014**, *84*, 29–36. [CrossRef]
23. Gaebele, D.T.; Magana, M.E.; Brekken, T.K.A.; Sawodny, O. State space model of an array of oscillating water column wave energy converters with inter-body hydrodynamic coupling. *Ocean. Eng.* **2020**, *195*, 106668. [CrossRef]
24. Kelly, T.; Dooley, T.; Campbell, J.; Ringwood, J. Modelling and Results for an Array of 32 Oscillating Water Columns. *Ewtec Proc.* **2013**. Available online: http://eprints.maynoothuniversity.ie/6788/ (accessed on 29 May 2022).
25. Lamont-Kane, P. Physical and Numerical Modelling of Wave Energy Converter Arrays. Ph.D. Thesis, Queen's University Belfast, Faculty of Engineering and Physical Sciences, Belfast, UK, 2015.
26. Doyle, S.; Aggidis, G.A. Experimental investigation and performance comparison of a 1 single OWC, array and M-OWC. *Renew. Energy* **2020**, *168*, 365–374. [CrossRef]
27. Doyle, S. Experimental and Numerical Investigation into the Energy Conversion Process in Single and Multi Chamber Oscillating Water Column Wave Energy Converters. Ph.D. Thesis, Lancaster University, Lancaster, UK, 2021.
28. Budal, K.; Falnes, J.; Kyllingstad, A.; Oltedal, G. Experiments with point absorbers. In Proceedings of the First Symposium on Wave Energy Utilization, Gothenburg, Sweden, 30 October–1 November 1979; pp. 253–282.
29. Count, B.M.; Jefferys, E.R. Wave power, the primary interface. In Proceedings of the 13th Symp. Naval Hydrodynamics, Tokyo, Japan, 6–10 October 1980; pp. 1–10.
30. Stallard, T.; Stansby, P.K.; Williamson, A.J. An experimental study of closely spaced point absorber arrays. In Proceedings of the International Offshore and Polar Engineering Conference, Vancouver, BC, Canada, 6–11 July 2008.
31. Thomas, S.; Weller, S.; Stallard, T. Float response within an array: Numerical and experimental comparison. In Proceedings of the 2nd International Conference on Ocean Energy (ICOE), Brest, France, 15–17 October 2008; Volume 1517.
32. Alexandre, A.; Stallard, T.; Stansby, P.K. Transformation of wave spectra across a line of wave devices. In Proceedings of the 8th European Wave and Tidal Energy Conference (EWTEC), Uppsala, Sweden, 7–10 September 2009.
33. Weller, S.D.; Stallard, T.; Stansby, P. Experimental measurements of irregular wave interaction factors in closely spaced arrays. *IET Renew. Power Gener.* **2010**, *4*, 628–637. [CrossRef]
34. Weller, S.D. Wave Energy Extraction from Device Arrays: Experimental Investigation in a Large Wave Facility. Ph.D. Thesis, University of Manchester, Faculty of Engineering and Physical Sciences, Manchester, UK, 2010.
35. Manchester University. Manchester Bobber Array. 2008. Available online: https://personalpages.manchester.ac.uk/staff/robert.j.brown/Default_files/Manchester_Bobber.htm (accessed on 12 August 2021).
36. Child, B.; Laporte Weywada, P. Verification and validation of a wave farm planning tool. In Proceedings of the 10th European Wave and Tidal Energy Conference Series-EWTEC, Aalborg, Denmark, 2–5 September 2013.
37. Folley, M.; Whittaker, T. Preliminary Cross-Validation of Wave Energy Converter Array Interactions. In Proceedings of the International Conference on Offshore Mechanics and Arctic Engineering–OMAE, Nantes, France, 9–14 June 2013; Volume 10837.
38. Lamont-Kane, P.; Folley, M.; Whittaker, T. Investigating Uncertainties in Physical Testing of Wave Energy Converter Arrays. In Proceedings of the 10th European Wave and Tidal Energy Conference Series-EWTEC, Aalborg, Denmark, 2–5 September 2013.
39. Mackay, E.; Cruz, J.; Livingstone, M.; Arnold, P. Validation of a Time-Domain Modelling Tool for Wave Energy Converter Arrays. In Proceedings of the 10th European Wave and Tidal Energy Conference, Aalborg, Denmark, 2–5 September 2013.
40. Ruiz, P.M.; Ferri, F.; Kofoed, J.P. Experimental Validation of a Wave Energy Converter Array Hydrodynamics Tool. *Sustainability* **2017**, *9*, 115 . [CrossRef]
41. Wave Star A/S. Wavestar. 2013. Available online: http://wavestarenergy.com/ (accessed on 15 June 2022).
42. Boere, R.; Goudswaard, R.; Schneider, T.; van Vlijmen, B. Interaction of Ocean Wave Energy Converters. Bachelor Thesis, TU Delft, Delft, The Netherlands, 2018.
43. Do, H.T.; Dang, T.D.; Ahn, K.K. A multi-point-absorber wave-energy converter for the stabilization of output power. *Ocean. Eng.* **2018**, *161*, 337–349. [CrossRef]
44. Binh, P.C.; Tri, N.M.; Dung, D.T.; Ahn, K.K.; Kim, S.J.; Koo, W. Analysis, design and experiment investigation of a novel wave energy converter. *IET Gener. Transm. Distrib.* **2015**, *10*, 460–469. [CrossRef]
45. Giassi, M.; Engström, J.; Isberg, J.; Göteman, M. Comparison of Wave Energy Park Layouts by Experimental and Numerical Methods. *J. Mar. Sci. Eng.* **2020**, *8*, 750. [CrossRef]
46. Thomas, S.; Giassi, M.; Göteman, M.; Hann, M.; Ransley, E.; Isberg, J.; Engström, J. Performance of a Direct-Driven Wave Energy Point Absorber with High Inertia Rotatory Power Take-off. *Energies* **2018**, *11*, 2332. [CrossRef]
47. Moreno, E.C.; Stansby, P. The 6-float wave energy converter M4: Ocean basin tests giving capture width, response and energy yield for several sites. *Renew. Sustain. Energy Rev.* **2019**, *104*, 307–318. [CrossRef]
48. Stansby, P.; Moreno, E.C.; Stallard, T.; Maggi, A. Three-float broad-band resonant line absorber with surge for wave energy conversion. *Renew. Energy* **2015**, *78*, 132–140. [CrossRef]
49. Stansby, P.; Moreno, E.C.; Stallard, T. Capture width of the three-float multi-mode multi-resonance broadband wave energy line absorber M4 from laboratory studies with irregular waves of different spectral shape and directional spread. *J. Ocean Eng. Mar. Energy* **2015**, *1*, 287–298. [CrossRef]
50. Santo, H.; Taylor, P.H.; Stansby, P.K. The performance of the three-float M4 wave energy converter off Albany, on the south coast of western Australia, compared to Orkney (EMEC) in the U.K. *Renew. Energy* **2020**, *146*, 444–459. [CrossRef]

51. Liao, Z.; Stansby, P.; Li, G.; Moreno, E.C. High-Capacity Wave Energy Conversion by Multi-Float, Multi-PTO, Control and Prediction: Generalized State-Space Modelling With Linear Optimal Control and Arbitrary Headings. *IEEE Trans. Sustain. Energy* **2021**, *12*, 2123–2131. [CrossRef]
52. Stansby, P.; Moreno, E.C.; Stallard, T. Large capacity multi-float configurations for the wave energy converter M4 using a time-domain linear diffraction model. *Appl. Ocean. Res.* **2017**, *68*, 53–64. [CrossRef]
53. Kamarlouei, M.; Gaspar, J.F.; Calvario, M.; Hallak, T.S.; Mendes, M.J.G.C.; Thiebaut, F.; Guedes Soares, C. Experimental analysis of wave energy converters concentrically attached on a floating offshore platform. *Renew. Energy* **2020**, *152*, 1171–1185. [CrossRef]
54. Sun, K.; Yang, Y.; Zheng, X.; Cui, L.; Zhao, C.; Liu, M.; Rao, X. Experimental investigation of semi-submersible platform combined with point-absorber array. *Energy Convers. Manag.* **2021**, *245*, 114623. [CrossRef]
55. Principle Power. WindFloat. 2022. Available online: https://www.principlepower.com/windfloat (accessed on 15 June 2022).
56. Beatty, S.; Ferri, F.; Bocking, B.; Kofoed, J.P.; Buckham, B. Power Take-Off Simulation for Scale Model Testing of Wave Energy Converters. *Energies* **2017**, *10*, 973. [CrossRef]
57. Windt, C.; Davidson, J.; Ringwood, J. High-fidelity numerical modelling of ocean wave energy systems: A review of computational fluid dynamics-based numerical wave tanks. *Renew. Sustain. Energy Rev.* **2018**, *93*, 610–630. [CrossRef]
58. García-Violini, D.; Peña Sanchez, Y.; Faedo, N.; Windt, C.; Ferri, F.; Ringwood, J.V. Experimental implementation and validation of a broadband LTI energy-maximising control strategy for the Wavestar device. *IEEE Trans. Control. Syst. Technol.* **2020**, *29*, 2609–2621. [CrossRef]
59. Bacelli, G.; Ringwood, J. Constrained control of arrays of wave energy devices. *Int. J. Mar. Energy* **2013**, *3–4*, 53–69. [CrossRef]
60. De Backer, G.; Vantorre, M.; Frigaard, P.; Beels, C.; De Rouck, J. Bottom slamming on heaving point absorber wave energy devices. *J. Mar. Sci. Technol.* **2010**, *15*, 119–130. [CrossRef]
61. Giorgi, G.; Ringwood, J.V. Nonlinear Froude-Krylov and viscous drag representations for wave energy converters in the computation/fidelity continuum. *Ocean. Eng.* **2017**, *141*, 164–175. [CrossRef]
62. Child, B.; Cruz, J.; Livingstone, M. The development of a tool for optimising of arrays of wave energy converters. In Proceedings of the 9th European Wave and Tidal Energy Conference, Southampton, UK, 5–9 September 2011.
63. Shadman, M.; Estefen, S.F.; Rodriguez, C.A.; Nogueira, I.C.M. A geometrical optimization method applied to a heaving point absorber wave energy converter. *Renew. Energy* **2017**, *115*, 533–546. [CrossRef]
64. Bacelli, G.; Spencer, S.J.; Patterson, D.C.; Coe, R.G. Wave tank and bench-top control testing of a wave energy converter. *Appl. Ocean. Res.* **2019**, *86*, 351–366. [CrossRef]
65. Troch, P.; Stratigaki, V.; Devriese, P.; Kortenhaus, A.; De Maeyer, J.; Monballiu, J.; Toorman, E.; Rawoens, P.; Vanneste, D.; Suzuki, T.; et al. Design Features of the Upcoming Coastal and Ocean Basin in Ostend, Belgium. 2018. Available online: https://icce-ojs-tamu.tdl.org/icce/index.php/icce/article/view/8721 (accessed on 29 May 2022).
66. Cargo, C.J.; Plummer, A.R.; Hillis, A.J.; Schlotter, M. Determination of optimal parameters for a hydraulic power take-off unit of a wave energy converter in regular waves. *Proc. IMechE Part A J. Power Energy* **2011**, *226*, 98–111. [CrossRef]
67. Verbrugghe, T. openWEC: Open Source Wave Energy Converter (WEC) Simulation Tool. Ghent University. 2018. Available online: https://users.ugent.be/~tverbrug/ (accessed on 2 June 2022).
68. OAV. OAV Air Bearing Product Book & Design Guide: Where Aerospace Techonology Meets Air Bearing Systems. 2021. Available online: https://www.oavco.com/brochures (accessed on 7 July 2021).
69. Beckhoff Automation. Beckhoff New Automation Technology, Operation Instructions, AM8000 and AM8500: Synchronous Servomotors, Version 4.9. 2022. Available online: https://download.beckhoff.com/download/document/motion/am8000-am8500-ba-en.pdf (accessed on 24 June 2022).
70. Coe, R.G.; Bacelli, G.; Forbush, D. A practical approach to wave energy modeling and control. *Renew. Sustain. Energy Rev.* **2021**, *142*, 110791. [CrossRef]
71. Faedo, N.; Carapellese, F.; Pasta, E.; Mattiazzo, G. On the principle of impedance-matching for underactuated wave energy harvesting systems. *Appl. Ocean. Res.* **2022**, *118*, 102958. [CrossRef]